



OPEN ACCESS

EDITED BY

Seth Frieze,
University of Vermont Cancer Center,
United States

REVIEWED BY

Georgia Tsagkogeorga,
STORM Therapeutics Ltd.,
United Kingdom
Michael Vandewege,
North Carolina State University,
United States

*CORRESPONDENCE

Jie Wang,

✉ wangjie@cib.ac.cn

Guangpu Zhang,

✉ zgp1122@outlook.com

Rachel Lockridge Mueller,

✉ rlm@colostate.edu

SPECIALTY SECTION

This article was submitted to
Epigenomics and Epigenetics,
a section of the journal
Frontiers in Cell and Developmental
Biology

RECEIVED 15 December 2022

ACCEPTED 09 February 2023

PUBLISHED 24 February 2023

CITATION

Wang J, Yuan L, Tang J, Liu J, Sun C,
Itgen MW, Chen G, Sessions SK, Zhang G
and Mueller RL (2023), Transposable
element and host silencing activity in
gigantic genomes.
Front. Cell Dev. Biol. 11:1124374.
doi: 10.3389/fcell.2023.1124374

COPYRIGHT

© 2023 Wang, Yuan, Tang, Liu, Sun, Itgen,
Chen, Sessions, Zhang and Mueller. This is
an open-access article distributed under
the terms of the [Creative Commons
Attribution License \(CC BY\)](https://creativecommons.org/licenses/by/4.0/). The use,
distribution or reproduction in other
forums is permitted, provided the original
author(s) and the copyright owner(s) are
credited and that the original publication
in this journal is cited, in accordance with
accepted academic practice. No use,
distribution or reproduction is permitted
which does not comply with these terms.

Transposable element and host silencing activity in gigantic genomes

Jie Wang^{1*}, Liang Yuan², Jiaying Tang^{1,3}, Jiongyu Liu¹,
Cheng Sun⁴, Michael W. Itgen⁵, Guiying Chen³,
Stanley K. Sessions⁶, Guangpu Zhang^{1,3*} and
Rachel Lockridge Mueller^{5*}

¹CAS Key Laboratory of Mountain Ecological Restoration and Bioresource Utilization & Ecological Restoration and Biodiversity Conservation Key Laboratory of Sichuan Province, Chengdu Institute of Biology, Chinese Academy of Sciences, Chengdu, Sichuan, China, ²School of Life Sciences, Xinjiang Normal University, Urumqi, China, ³College of Life Sciences, Sichuan Normal University, Chengdu, China, ⁴College of Life Sciences, Capital Normal University, Beijing, China, ⁵Department of Biology, Colorado State University, Fort Collins, CO, United States, ⁶Biology Department, Hartwick College, Oneonta, NY, United States

Transposable elements (TEs) and the silencing machinery of their hosts are engaged in a germline arms-race dynamic that shapes TE accumulation and, therefore, genome size. In animal species with extremely large genomes (>10 Gb), TE accumulation has been pushed to the extreme, prompting the question of whether TE silencing also deviates from typical conditions. To address this question, we characterize TE silencing via two pathways—the piRNA pathway and KRAB-ZFP transcriptional repression—in the male and female gonads of *Ranodon sibiricus*, a salamander species with a ~21 Gb genome. We quantify 1) genomic TE diversity, 2) TE expression, and 3) small RNA expression and find a significant relationship between the expression of piRNAs and TEs they target for silencing in both ovaries and testes. We also quantified TE silencing pathway gene expression in *R. sibiricus* and 14 other vertebrates with genome sizes ranging from 1 to 130 Gb and find no association between pathway expression and genome size. Taken together, our results reveal that the gigantic *R. sibiricus* genome includes at least 19 putatively active TE superfamilies, all of which are targeted by the piRNA pathway in proportion to their expression levels, suggesting comprehensive piRNA-mediated silencing. Testes have higher TE expression than ovaries, suggesting that they may contribute more to the species' high genomic TE load. We posit that apparently conflicting interpretations of TE silencing and genomic gigantism in the literature, as well as the absence of a correlation between TE silencing pathway gene expression and genome size, can be reconciled by considering whether the TE community or the host is currently “on the attack” in the arms race dynamic.

KEYWORDS

TE expression, TE diversity, TE silencing, piRNA pathway, genome size evolution, salamander, KRAB-ZFP, *Ranodon sibiricus*

1 Introduction

Transposable elements (TEs) are DNA sequences that can mobilize throughout the genomes of their hosts, typically replicating as part of the transposition life cycle (Doolittle and Sapienza, 1980; Orgel and Crick, 1980; Wicker et al., 2007). TEs are an ancient and diverse class of sequences, encompassing a range of replication

mechanisms that rely on both TE- and host-encoded enzymatic machinery (Bourque et al., 2018). Eukaryotic genomes contain a substantial yet variable number of TEs; they make up well over half of the human genome, up to 85% of the maize genome (Haberer et al., 2005), yet only ~0.1% of the yeast *Pseudozyma antarctica* genome (de Koning et al., 2011; Castanera et al., 2017; Jiao et al., 2017). TE abundance is one of the major determinants of overall genome size, which ranges from ~0.002 Gb to ~150 Gb across eukaryotes and from ~0.4 Gb to ~130 Gb across vertebrates (Rodriguez and Arkhipova, 2018; Gregory, 2022). The mechanistic and evolutionary forces shaping TE abundance and, thus, genome size remain incompletely understood.

Individual TE insertions have a range of effects on host fitness; the majority are effectively neutral or slightly deleterious, while smaller proportions are either harmful (or lethal) on the one hand or adaptive on the other (Arkhipova, 2018; Almeida et al., 2022). For example, at least 120 human diseases have been attributed to the effects of *de novo* TE insertions, but so have classic adaptive traits including industrial melanism and the mammalian placenta (Hancks and Kazazian, 2016; Hof et al., 2016; Senft and Macfarlan, 2021). The likelihood of a novel TE insertion having an extreme effect on the host phenotype depends on properties of the host genome including gene density, which affects the probability of a new insertion disrupting a functional protein-coding or regulatory sequence (Medstrand et al., 2002).

In response to TEs' mutagenic properties, eukaryotes have evolved multiple mechanisms to silence their activity, particularly in the germline and early embryo where TE effects on host fitness are the most pronounced (Almeida et al., 2022). Some mechanisms act by transcriptionally silencing TE loci through targeted deposition of chromatin modifications (e.g., methylation of cytosines on DNA, or H3K9 methylation of histone proteins) (Deniz et al., 2019). Other mechanisms act post-transcriptionally, targeting TE transcripts for destruction in the cytoplasm before they can complete the replicative life cycle and generate a novel genomic TE insertion (Czech and Hannon, 2016).

In multicellular animals, TE silencing in the germline and during early embryogenesis is carried out by the piRNA pathway, a small RNA pathway that relies on RNA-induced silencing complexes (RISC) composed of PIWI proteins and associated guide piRNAs that identify TE transcripts by base complementarity (Aravin et al., 2006; Ozata et al., 2019; Iwakawa and Tomari, 2022). In the nucleus, piRNA-PIWI complexes identify chromatin-associated nascent TE transcripts, inducing transcriptional silencing of the genomic TE locus through recruitment of DNA methyltransferases and histone methyltransferases to establish a repressive chromatin structure (Aravin et al., 2008; Czech et al., 2018). In the cytoplasm, piRNA-PIWI complexes identify mature TE transcripts and cleave them between nucleotide positions 10 and 11 of the guide piRNA (Reuter et al., 2011; Iwasaki et al., 2015). The cleaved fragments of TE mRNA induce the production of more TE-targeting piRNAs through a feed-forward loop called the ping-pong cycle, which amplifies the cell's post-transcriptional TE silencing response (Brennecke

et al., 2007; Gunawardane et al., 2007; Castel and Martienssen, 2013). Although present in both males and females, there are sex-specific differences in activity of the piRNA pathway, which may be associated with sex-biased contributions to overall genomic TE load (Saint-Leandre et al., 2020).

In tetrapods, lungfishes, and coelacanths, TE silencing is also carried out by a large family of transcriptional modulators called the Krüppel-associated box domain-containing zinc-finger proteins (KRAB-ZFPs) (Imbeault et al., 2017). These proteins include an array of zinc fingers, each of which binds short DNA sequences such that, together, they confer specificity to individual TE families (Thomas and Schneider, 2011). These proteins also include the KRAB domain, which recruits KAP1/TRIM28 and, in turn, a silencing complex of proteins including the nucleosome remodeling deacetylase complex (NuRD) that establish a repressive chromatin structure at TE loci (Ecco et al., 2017). The NuRD complex is similarly recruited for TE transcriptional silencing by the piRNA pathway (Wang et al., 2023).

Although these TE silencing pathways are broadly conserved phylogenetically and functionally critical for maintaining genome integrity, they nonetheless evolve (Parhad and Theurkauf, 2019; Gutierrez et al., 2021). Our work is motivated by the hypothesis that their evolution contributes to variation in TE content, and therefore overall genome size, across the tree of life (Mueller, 2017). Species that are extreme genome size outliers provide a powerful test of this hypothesis, as they are predicted to harbor strong signatures of divergent TE silencing compared with genomes of more typical size.

Among vertebrates, extreme genome expansion through TE accumulation evolved independently in salamanders and in lungfishes, with large increases in both lineages occurring over 200 million years ago (Liedtke et al., 2018; Meyer et al., 2021). Salamanders are one of the three clades of living amphibians; there are 775 extant species, and haploid genome sizes range from 9 to 120 Gb, reflecting ongoing genome size evolution (AmphibiaWeb, 2022; Gregory, 2022). Amphibians also include some of the smallest vertebrate genomes; the ornate burrowing frog *Platyplectrum ornatum* and the New Mexico spadefoot toad *Spea multiplicata* have genome sizes of 1.06 and 1.09 Gb, respectively (Lamichhaney et al., 2021; Gregory, 2022). Lungfishes are the sister taxon to tetrapods; there are six extant species, and haploid genome size estimates range from 40 Gb to 130 Gb (Meyer et al., 2021).

To date, several studies have begun to explore the relationship between TE silencing and genome size among vertebrates. At the smaller extremes, studies of frogs and fish with tiny genomes (≤ 1 Gb) revealed at least one additional duplicate copy of a PIWI gene, suggesting increased activity of the piRNA pathway in silencing TEs in genomes that have undergone size reduction (Malmström et al., 2018; Lamichhaney et al., 2021). At the larger extremes, the data reveal a more complex picture; the Australian and African lungfish genomes (*Neoceratodus forsteri* and *Protopterus annectens*, ≥ 40 Gb) show neither gains nor losses of PIWI or related genes (Biscotti et al., 2017; Meyer et al., 2021). However, the African lungfish genome includes far more KRAB domains than other vertebrate genomes, suggesting a copy-number-based increase in

TABLE 1 Repeat contigs (≥ 100 bp) identified by different methods/software in the PiRATE pipeline (Berthelier et al., 2018).

TE-mining method	Software	Repeats clustered at 100% identify
Similarity-based	RepeatMasker	75,381 (68.6%)
	TE-HMMER	3,108 (2.8%)
Structure-based	HelSearch	1 (0.0%)
	LTR harvest	84 (0.1%)
	MGEScan-non-LTR	0
	MITE hunter	7 (0.0%)
	SINE finder	48 (0.0%)
Repetitiveness-based	TEdenovo	306 (0.3%)
	RepeatScout	3,671 (3.3%)
Repeat-building-based	dnaPipeTE	24,090 (21.9%)
	RepeatModeler	3,213 (2.9%)
In total		109,909 (100%)

activity. In contrast, the genome of the Mexican axolotl salamander *Ambystoma mexicanum* (~32 Gb) (Nowoshilow et al., 2018) contains a comparable number of KRAB domains to mammalian and non-avian reptile genomes, suggesting no similar increase in this TE silencing activity (Wang et al., 2021b).

Transcriptomic data reveal a similarly mixed picture: for some piRNA pathway genes, germline expression is higher in salamanders (represented by the fire-bellied newt *Cynops orientalis*, ~44 Gb) than in the African lungfish, whereas for other genes, the pattern is reversed; comparisons with genomes of more typical size (coelacanth *Latimeria menadoensis* and zebrafish *Danio rerio*) show patterns of both higher and lower germline expression of TE silencing genes in the species with gigantic genomes (Biscotti et al., 2017; Carducci et al., 2021). Small RNA sequence data from the gonads of the northern dusky salamander *Desmognathus fuscus* (~15 Gb) reveal lower percentages of TE-mapping piRNAs than are found in smaller genomes, suggesting a less comprehensive TE-targeting piRNA pool in the gigantic genome (Madison-Villar et al., 2016). Taken together, these inconsistent patterns reveal that the relationship between TE silencing pathway activity and genome size evolution remains incompletely understood, and that integrating genomic, transcriptomic, and small RNA analysis is critical for a complete picture.

Here we present a detailed analysis of TEs and germline TE silencing activity in the central Asian salamander *Ranodon sibiricus*—a range-restricted species endemic to China and Kazakhstan—adding both phylogenetic (family Hynobiidae) and genome size (~21 Gb) diversity to the small but growing dataset on TE silencing in gigantic genomes (AmphibiaWeb, 2022; Gregory, 2022). We quantify the expression of TEs in the male and female gonads, and we complement this data with analyses of the genomic TE landscape and TE amplification histories to reveal what TE superfamilies are active in the *R. sibiricus* genome. We quantify small RNAs expressed in male and female gonads and test whether small RNAs targeting TEs for silencing are expressed and amplified in proportion to TE expression. We quantify the relative expression

of genes encoding proteins from 2 TE silencing pathways—piRNA and KRAB-ZFP. Finally, we extend these latter analyses to other vertebrates with a range of genome sizes to test for changes in TE silencing accompanying extreme increases in genome size.

2 Results

2.1 The genome of *R. sibiricus* contains diverse known, active TE superfamilies

We estimated the haploid genome size of *R. sibiricus* to be 17 Gb; averaging our result with published estimates (22.3 or 24.8 Gb; Gregory, 2022) yields 21.3 Gb. We used the PiRATE pipeline (Berthelier et al., 2018), which was designed to mine and classify repeats from low-coverage genomic shotgun data in taxa that lack genomic resources. The pipeline yielded 109,909 repeat contigs (Table 1). RepeatMasker mined the most repeats (75,381 out of 109,909; 68.6%), followed by dnaPipeTE (21.9%), RepeatScout (3.3%), RepeatModeler (2.9%), and TE-HMMER (2.8%). TEdenovo, LTRharvest, HelSearch, SINE-Finder, and MITE-Hunter found few repeats, and MGEScan-non-LTR found none.

Repeat contigs were annotated as TEs to the levels of order and superfamily in Wicker's hierarchical classification system (Wicker et al., 2007), modified to include several recently discovered TE superfamilies, using PASTEC (Hoede et al., 2014). Of the 109,909 identified repeat contigs, 1,088 were filtered out as potential chimeras, 275 were classified as potential multiple-copy host genes, and 54,221 (49.33%) were classified as known TEs (Table 2), representing 23 superfamilies in eight orders as well as retrotransposon and transposon derivatives.

To calculate the proportion of different repeats in the genome, shotgun reads were masked with RepeatMasker using two *R. sibiricus*-derived repeat libraries: excluding or including unknown repeats. This comparison revealed how many reads were sufficiently similar to known TEs to be masked by them when unknown repeat

TABLE 2 Classification of repeat contigs (modified from Wicker 2007) and summary of repeats detected in the genome.

Order	Superfamily	Percent of genome ^a	Genomic contigs (100% identical)	Genomic contigs (95% identical)	Genomic contigs (80% identical)	Average genomic contig length (100% identical) (bp)	Longest genomic contig length (bp)	Transcriptome contigs (80% identical)	Expression level in ovaries (TPM)	Expression level in testes (TPM)
Class I - Retrotransposons - Autonomous										
LTR	<i>Gypsy</i>	3.85-6.50	5,985	5,464	3,835	548	7,587	2,057	827	3,024
	<i>ERV</i>	0.41-0.43	413	394	264	593	11,567	321	392	694
	<i>Copia</i>	0.10-0.25	23	21	19	592	1,353	27	31	26
	<i>Bel-Pao</i>	0.05	12	7	2	575	766	-	-	-
	<i>Retrovirus</i>	-	3	2	2	1,375	1,719	10	1	10
	<i>THE1</i>	-	4	4	3	491	674	-	-	-
	<i>Unknown LTR</i>	-	4	4	4	469	955	-	-	-
DIRS	<i>DIRS</i>	4.44-5.95	8,087	7,821	3,844	379	4,266	4,844	5,427	11,962
PLE	<i>Penelope</i>	0.09-0.12	482	462	376	407	3,208	460	123	352
LINE	<i>Jockey</i>	9.69-12.12	25,276	23,361	13,287	426	3,625	11,622	6,206	15,535
	<i>L1</i>	5.04-6.62	10,189	8,997	5,941	672	6,546	8,241	2,954	7,610
	<i>RTE</i>	0.12-0.24	227	201	137	676	4,540	399	130	360
	<i>I</i>	0.09-0.17	32	25	10	905	3,858	48	42	125
	<i>R2</i>	-	-	-	-	-	-	1	-	1
	<i>Unknown LINE</i>	0.39-1.89	90	77	72	1,393	5,881	1	-	-
Class I - Retrotransposons - Non-autonomous										
SINE	<i>5S</i>	0.23-0.18	57	41	15	773	1,783	4	5	1
	<i>7SL</i>	-	43	41	15	243	450	2	1	-
	<i>tRNA</i>	-	22	22	22	273	403	-	-	-
	<i>Unknown SINE</i>	0.45-3.42	365	348	338	377	695	219	2,901	2,471
Retrotransposon Derivatives	<i>TRIM</i>	3.80-9.76	748	631	465	588	2,619	492	1,651	5,847
	<i>LARD</i>	0.15-0.73	45	37	35	2,834	8,148	153	515	2,643

(Continued on following page)

TABLE 2 (Continued) Classification of repeat contigs (modified from Wicker 2007) and summary of repeats detected in the genome.

Order	Superfamily	Percent of genome ^a	Genomic contigs (100% identical)	Genomic contigs (95% identical)	Genomic contigs (80% identical)	Average genomic contig length (100% identical) (bp)	Longest genomic contig length (bp)	Transcriptome contigs (80% identical)	Expression level in ovaries (TPM)	Expression level in testes (TPM)
Class II - DNA Transposons - Subclass 1										
TIR	<i>PIF-Harbinger</i>	2.98-4.22	1,164	1,014	434	411	5,169	416	575	1,359
	<i>hAT</i>	1.15-1.12	177	135	55	869	5,706	35	83	26
	<i>Tc1-Mariner</i>	0.18-0.63	73	40	24	1,025	3,781	20	58	87
	<i>PiggyBac</i>	0.05-0.08	9	8	6	1,087	1,956	6	21	15
	<i>MuDR</i>	-	3	3	3	266	417	13	4	10
	<i>CACTA</i>	-	2	2	2	645	846	3	2	1
	<i>ISL2EU</i>	-	-	-	-	-	-	1	18	16
	<i>Ginger</i>	-	-	-	-	-	-	4	10	6
	<i>Academ</i>	-	-	-	-	-	-	11	5	8
	<i>P</i>	-	-	-	-	-	-	1	1	1
	<i>Unknown TIR</i>	0.33-1.46	22	20	19	754	2,174	-	-	-
Transposon Derivatives	MITE	0.56-4.07	357	346	321	258	1,942	137	465	1,188
Class II - DNA Transposons - Subclass 2										
Maverick	<i>Maverick</i>	0.05	258	228	65	583	6,090	123	44	762
Helitron	<i>Helitron</i>	0.18-0.48	49	38	19	939	6,551	13	2	10
Total		34.38-60.54	54,221	49,794	29,634	489	11,567	29,684	22,494	42,200

^aThe first and second numbers were estimated including and excluding unknown repeats, respectively, from the repeat library. Transposable element superfamily names are italicized.

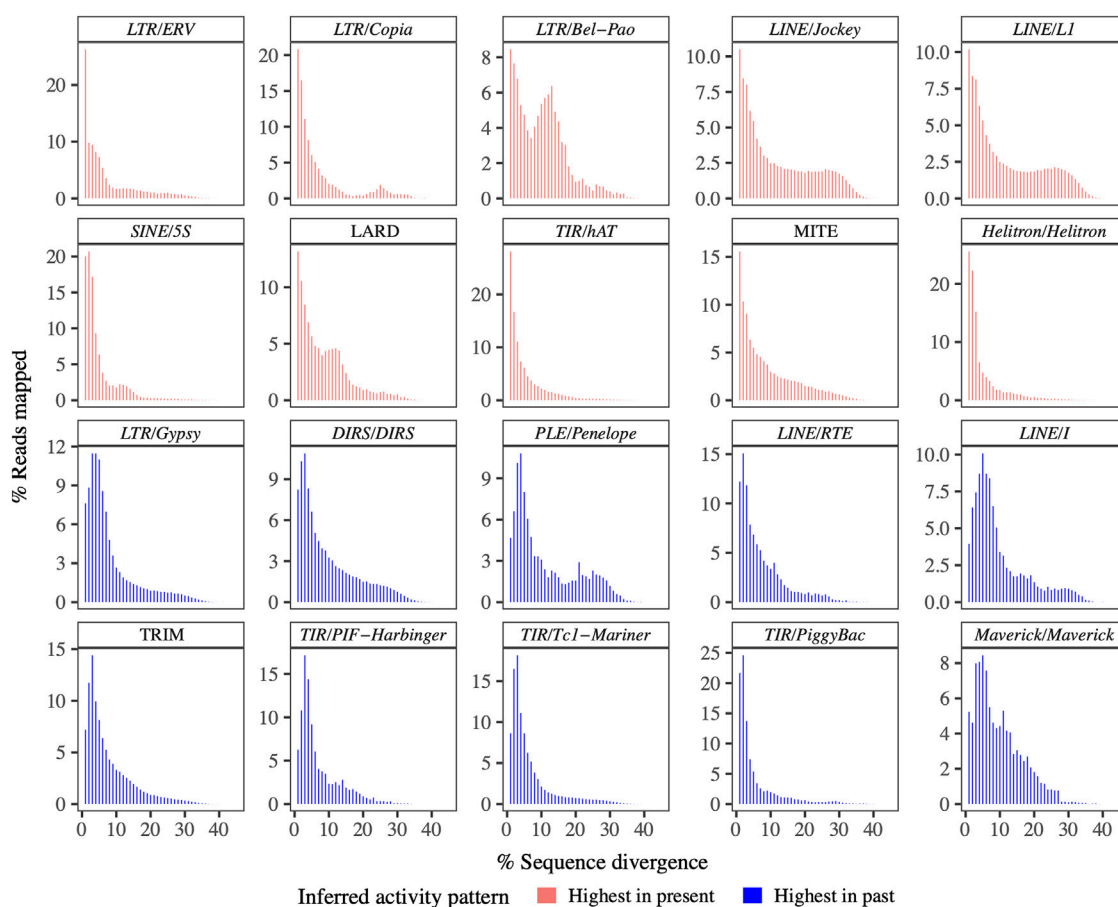


FIGURE 1

Amplification plots for TE superfamilies and derivatives. All of the amplification plots suggest current activity. Note that the y-axes differ in scale.

contigs were not available as a best-match option; it thus provides a rough approximation of the quantity of unknown repeats that were TE-derived, but divergent, fragmented, or otherwise unidentifiable by our pipeline (Wang et al., 2021a).

Class I TEs (retrotransposons) make up 28.90%–48.43% (unknown repeats included or excluded in the repeat library, respectively) of the *R. sibiricus* genome; they are over 4 times more abundant than Class II TEs (DNA transposons; 5.48%–12.11%). *LINE/Jockey* is the most abundant superfamily (9.69%–12.12% of the genome), followed by *LINE/L1* (5.04%–6.62%), *DIRS/DIRS* (4.44%–5.95%), *LTR/Gypsy* (3.85%–6.50%), and *TRIM* (3.80%–9.76%); all are retrotransposons or retrotransposon derivatives (Table 2). *TIR/PIF-harbinger* (2.98%–4.22%), *TIR/hAT* (1.12%–1.15%), and *MITE* (0.56%–4.07%) are the most abundant superfamilies of DNA transposons/transposon derivatives (Table 2). Overall repeat percentages are within the range of estimates for other amphibians with gigantic genomes (22%–68%), and the six most abundant TE superfamilies in *R. sibiricus* are frequently among the top six superfamilies in these other genomes (Sun et al., 2012; Sun and Mueller, 2014; Nowoshilow et al., 2018; Wang et al., 2021a; Haley and Mueller, 2022).

Diversity of the overall genomic TE community was measured using both Simpson's and Shannon diversity indices, considering TE

superfamilies as “species” and the total number of base pairs for each annotated superfamily as individuals per “species.” The Gini-Simpson Index (1-D) is 0.83, and the Shannon Index H is 1.92, similar to estimates of genomic diversity from other salamander species (Wang et al., 2021a; Haley and Mueller, 2022).

Seventeen superfamilies and three retrotransposon or transposon derivatives (each covering more than 0.05% of the genome) were selected for summaries of overall amplification history, generated by plotting the genetic distances between individual reads (representing TE loci) and the corresponding ancestral TE sequences as a histogram, with bins of 1%. All of the resulting distributions showed characteristics of ongoing or recent activity (i.e., presence of TE sequences <1% diverged from the ancestral sequence) (Figure 1).

Ten of these showed right-skewed, essentially monotonically decreasing distributions with a maximum or near-maximum at < 1% diverged from the ancestral sequence: *LTR/ERV*, *LTR/Copia*, *LTR/Bel-Pao*, *LINE/Jockey*, *LINE/L1*, *SINE/5S*, *LARD*, *TIR/hAT*, *MITE*, and *Helitron/Helitron*, suggesting TE superfamilies or derivatives that continue to be replicating today at their highest-ever rates of accumulation. In contrast, 10 TE superfamilies or derivatives showed right-skewed, uni- or multimodal distributions: *LTR/Gypsy*, *DIRS/DIRS*, *PLE/Penelope*, *LINE/I*, *LINE/RTE*, *TRIM*, *TIR/PIF-Harbinger*, *TIR/Tc1-Mariner*, *TIR/*

TABLE 3 Overall summary of transcriptome annotation and expression in each sex.

	No. of contigs expressed in ovaries (percentage of total contigs)	Summed TPM in ovaries (percentage of total expression)	No. of contigs expressed in testes (percentage of total contigs)	Summed TPM in testes (percentage of total expression)
Endogenous gene	51,647 (17.4%)	678,366 (67.8%)	58,041 (13.3%)	513,783 (51.4%)
Autonomous TE	26,358 (8.9%)	17,890 (1.8%)	41,421 (9.5%)	43,694 (4.4%)
Non-autonomous TE	1,700 (0.6%)	5,538 (0.6%)	2,348 (0.5%)	12,151 (1.2%)
Gene/autonomous TE	722 (0.2%)	2,618 (0.3%)	1,001 (0.2%)	5,748 (0.6%)
Gene/non-autonomous TE	168 (0.1%)	2,779 (0.3%)	189 (0.0%)	1,073 (0.1%)
Unannotated	215,508 (72.8%)	292,828 (29.3%)	334,533 (76.5%)	423,550 (42.4%)
Total	296,103 (100%)	1,000,029 (100%)	437,533 (100%)	999,999 (100%)

PiggyBac, and *Maverick/Maverick*. These 10 distributions suggest TE superfamilies that continue to be active today, but whose accumulation peaked at some point in the past.

2.2 Germline relative TE expression is higher in testes than ovaries, but is correlated with genomic abundance in the gonads of both sexes

Our *de novo* gonad transcriptome assembly yielded 510,439 contigs (N50 = 1,250 bp; min and max contig lengths = 201 bp and 28,590 bp; total assembly length = 362,097,394 bp). The BUSCO pipeline revealed the presence of 95.3% of core vertebrate genes and 89.8% of core tetrapod genes. 47,182 contigs were annotated as TEs (representing 28 superfamilies), 64,409 as endogenous genes (representing 28,283 different genes), and 1,257 as having both a TE and an endogenous gene; the majority of contigs (72%) remained unannotated.

Endogenous genes account for the majority of expression in the gonads of both sexes (68% and 51% of summed TPM in females and males, respectively), followed by unannotated contigs (29% and 42%). Relative expression of TEs is an order of magnitude lower than endogenous gene expression in both sexes (2.4% and 5.6%) (Table 3, Supplementary File S3); these expression levels are comparable to those seen in the gonads of vertebrates with typical (i.e., much smaller) genome sizes (Pasquesi et al., 2020). Nine superfamilies (*LTR/Retrovirus*, *LINE/R2*, *SINE/7SL*, *TIR/MuDR*, *TIR/CACTA*, *TIR/ISL2EU*, *TIR/Ginger*, *TIR/Academ*, *TIR/P*) were detected at low expression levels in the transcriptome but were not initially detected in the genomic data (Table 2); mapping the genomic reads to these transcriptome contigs with Bowtie2 identified an average of four reads per superfamily, indicating that they are non-silenced, extremely low frequency, genomic repeats. Because our analysis is focused on TE expression, and we were able to identify these superfamilies in the transcriptome data, the initial failure to identify these superfamilies in the genomic dataset does not influence downstream analysis. In contrast, only one superfamily (*LTR/Bel-Pao*) was detected in the genomic data but not in the transcriptome data. Overall, 19 superfamilies were identified both in the genomic contigs and transcriptome contigs.

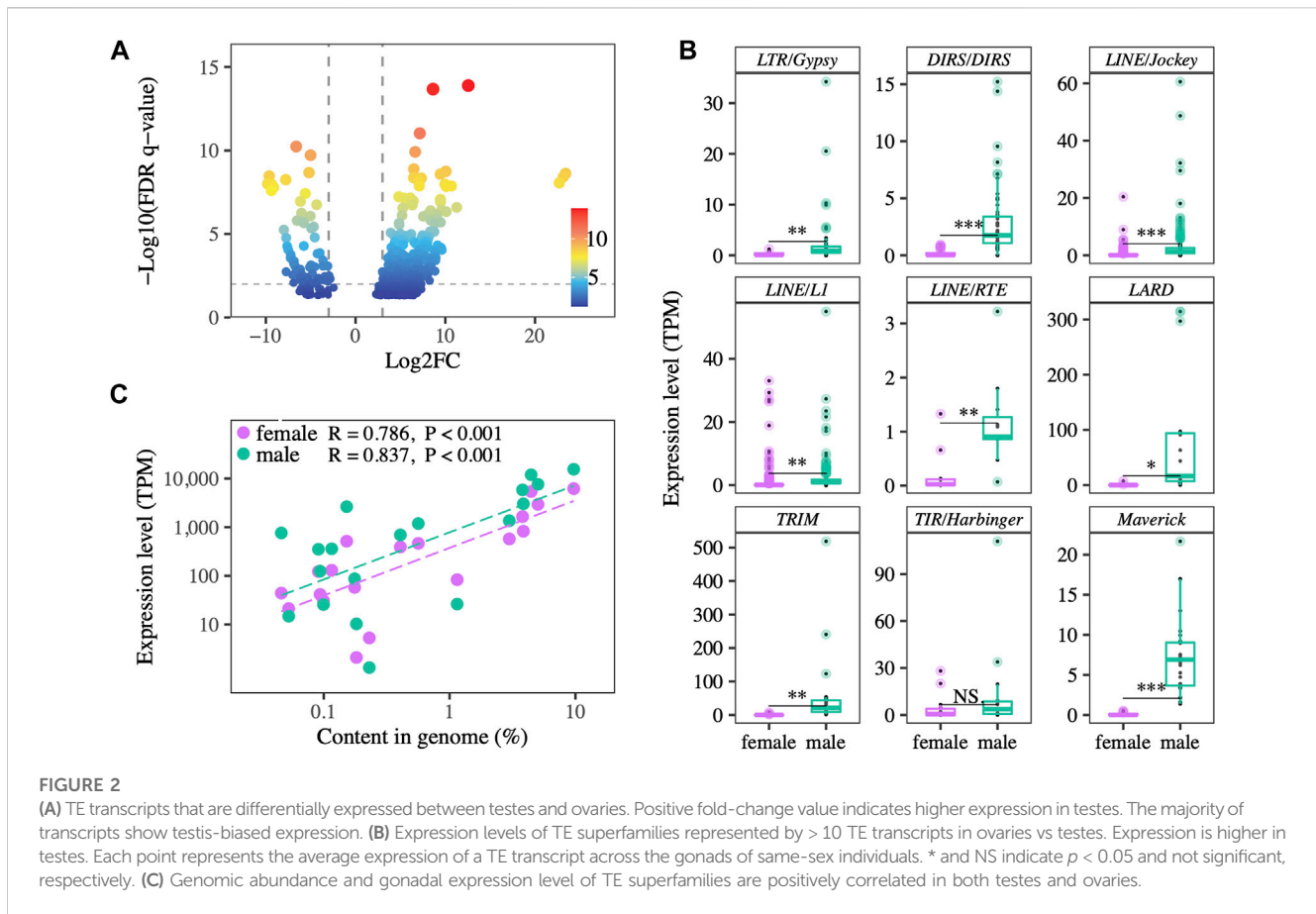
In ovaries, autonomous TEs account for 8.9% of the total transcriptome contigs and 1.8% of the overall transcripts (summed TPM = 17,890) (Table 3). Non-autonomous TEs account for only 0.6% of the total transcriptome contigs, but still represent 0.6% of the overall transcripts (summed TPM = 5,538). In testes, relative TE expression is more than double that seen in ovaries, with 4.4% and 1.2% of the overall gonad transcriptome accounted for by autonomous and non-autonomous TEs, respectively.

Differential expression analysis identified 780 contigs of 18 TE superfamilies as differently expressed between testes and ovaries. 678 TE transcripts were more highly expressed in testes, while only 102 TE transcripts were more highly expressed in ovaries (Figure 2A). Of the nine superfamilies with more than ten differentially expressed transcripts between testes and ovaries, eight of them showed significantly higher relative expression in testes than ovaries, and one showed a non-significant trend towards higher testis expression (Figure 2B). Across the 19 TE superfamilies detected in both the genomic and transcriptomic datasets, genomic abundance is positively correlated with overall relative expression both in ovaries ($R = 0.786$, $p < 0.001$) and testes ($R = 0.837$, $p < 0.001$), with testis relative expression higher overall (Figure 2C).

2.3 Expression of TE-mapping piRNAs correlates with TE expression in the gonads

In both testes and ovaries, the length distribution of small RNAs includes a peak at 29 nucleotides (Figure 3A), and sequences up to 30 nt show a strong 5'-U bias at the first nucleotide position, consistent with expectations for the piRNA pool (Figure 3B). In ovaries, there is a second peak at 22 nucleotides. The relative expression of putative piRNAs (25–30 nt) is lower in ovaries than in testes. In contrast, the relative expression of ~22 nt RNAs is higher in ovaries than in testes; 41%–59% of 22 nt RNAs correspond to known miRNAs in ovaries, versus 37%–41% in testes.

A higher percentage of total putative piRNAs map to TEs in ovaries than in testes; on average, 22.7% map in the antisense direction and 23.5% map in the sense direction in ovaries, and 11.0% map in the antisense direction and 10.1% map in the sense direction in testes. Considering unique putative piRNA sequences, 16.9% map in the



antisense direction and 17.1% map in the sense direction in ovaries, and 15.1% map in the antisense direction and 14.7% map in the sense direction in testes. Overall, more total putative piRNAs map to TEs in testes than ovaries, although the ranges overlap (1,264,088–3,045,727 in testis samples versus 897,586–2,503,814 in ovary samples) (Figure 3B).

In the gonads of both sexes, we identify a peak overlap length between TE-mapping sense and anti-sense piRNAs of 10 base pairs, consistent with ping-pong amplification of piRNAs in response to TE transcription (Figure 3C, Supplementary File S5). The strength of the ping-pong signal, indicated by the Z-scores of the 10-nt overlap, is greater in ovaries.

piRNA expression is correlated with TE expression, measured at the TE superfamily level, in both ovaries and testes (Figure 4A, Supplementary File S4), consistent with patterns observed in other species (Vandeweghe et al., 2016). At higher levels of TE expression, ovaries show a trend of having more piRNAs relative to TE expression level than testes. Ping-pong piRNA counts are also correlated with TE expression in ovaries and testes (Figure 4B), but the correlation with expression level is weaker, and testes have higher counts relative to TE expression than ovaries.

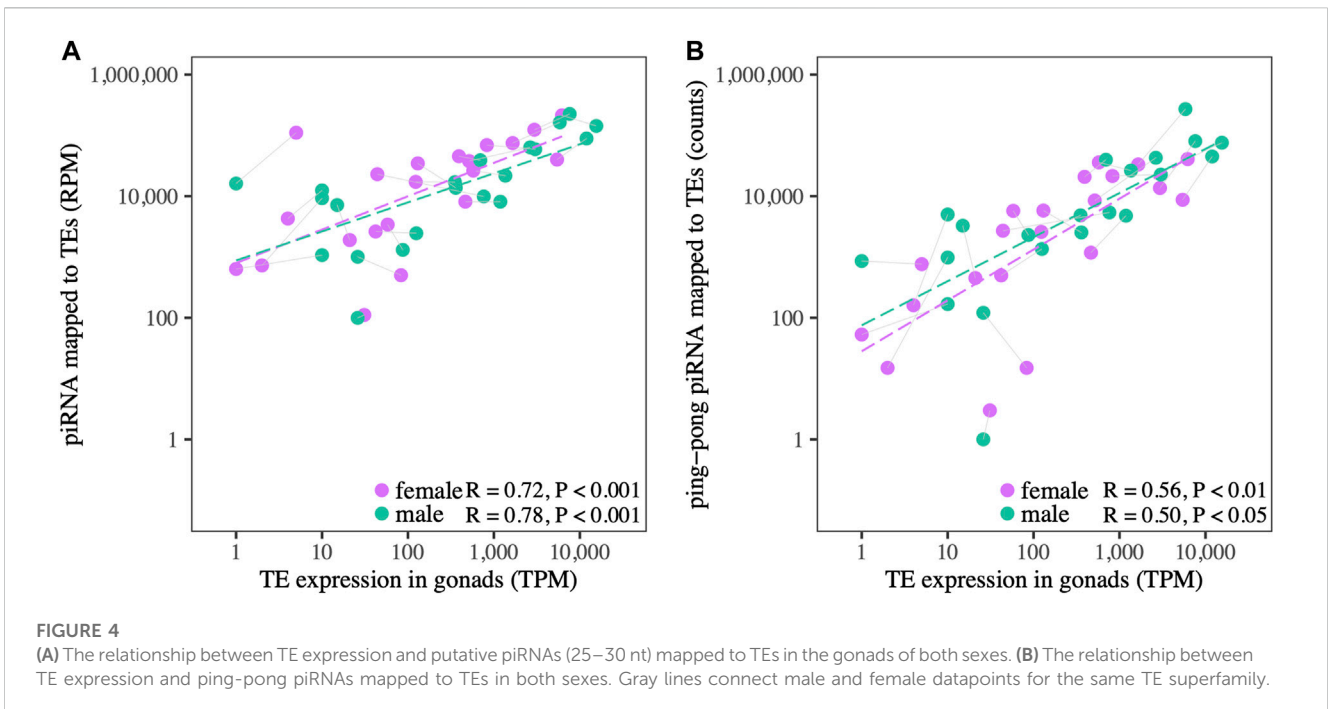
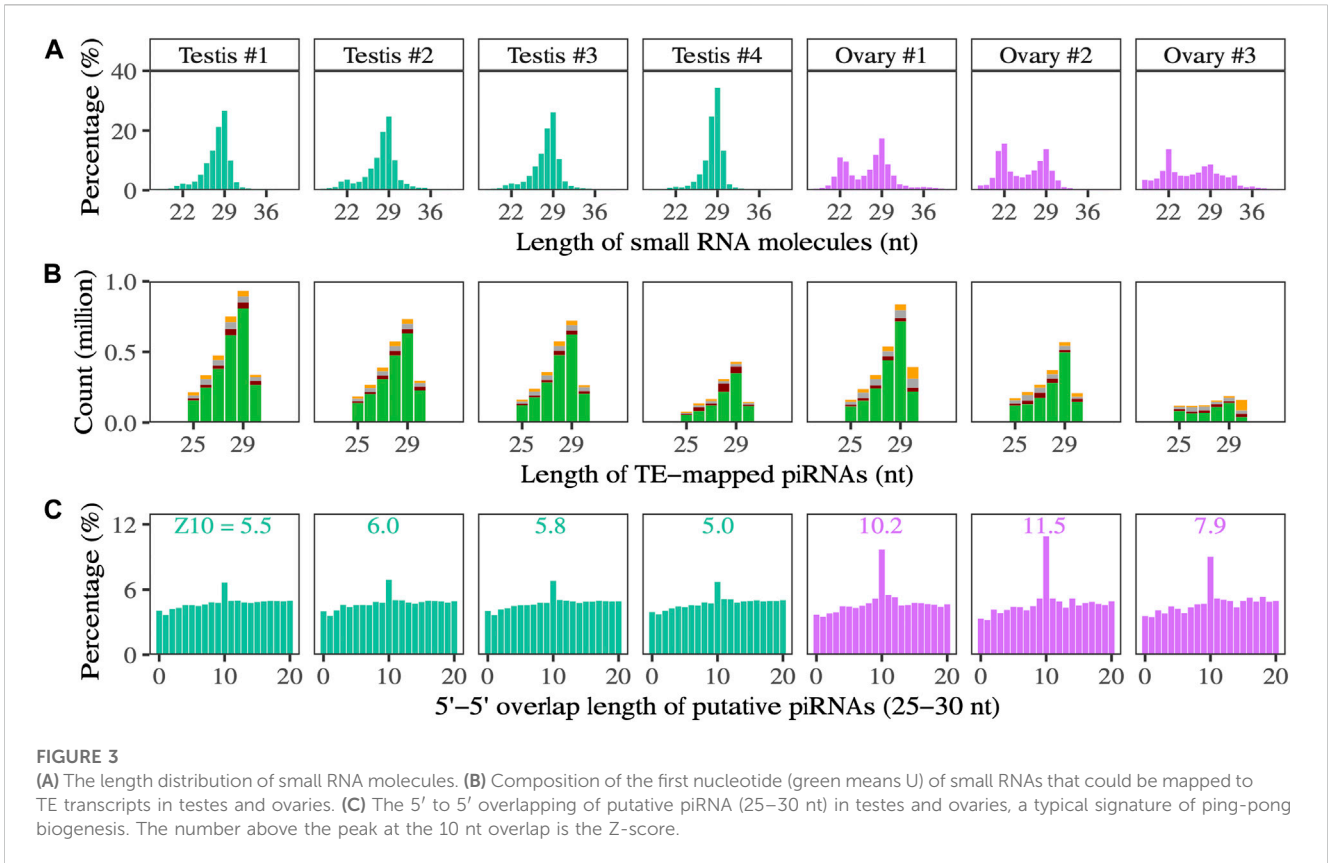
2.4 Germline expression of piRNA pathway genes is higher in testes in *R. sibiricus*, whereas KRAB-ZFP silencing and miRNA pathway genes are higher in ovaries

The expression of piRNA pathway genes in *R. sibiricus* is higher in testes than in ovaries, measured both relative to miRNA pathway

gene expression and as TPM (Figure 5; Supplementary Files S6,7). In contrast, the expression of genes establishing a repressive transcriptional environment (NuRD complex + related proteins) is comparable between the gonads of both sexes relative to miRNA pathway gene expression and slightly higher in ovaries measured as TPM. The expression of TRIM28 — which links KRAB-ZFP proteins to the NuRD complex + related proteins—is slightly higher in ovaries than testes relative to miRNA expression, yet miRNA pathway expression levels (TPM) are slightly higher in ovaries (consistent with higher miRNA expression, Figure 3; Supplementary Files S6,7). Taken together, these results suggest that male gonads may rely more heavily on piRNA machinery to recruit repressive transcriptional machinery, whereas female gonads may rely more heavily on KRAB-ZFP proteins to recruit repressive transcriptional machinery.

2.5 Relative expression of TE silencing pathways between testes and ovaries varies across species

Across species, higher piRNA pathway expression relative to miRNA pathway expression in testes is seen in the majority of taxa across the range of genome sizes; the exceptions are *Gallus gallus* and *P. annectens* (Figure 5, Supplementary File S6). Similarly, higher miRNA pathway expression in ovaries (TPM) is seen in all taxa except *G. gallus* and *D. rerio*, although the difference is not always as



pronounced as in *R. sibiricus* (Supplementary Files 7). *Platyplectrum ornatus*, *Anolis carolinensis*, and *C. orientalis* show the same pattern of TE silencing expression differences between testes and ovaries as

in *R. sibiricus*, with higher reliance on piRNA machinery in testes and higher reliance on KRAB-ZFP in ovaries. However, this pattern does not hold in other taxa (Figure 5).

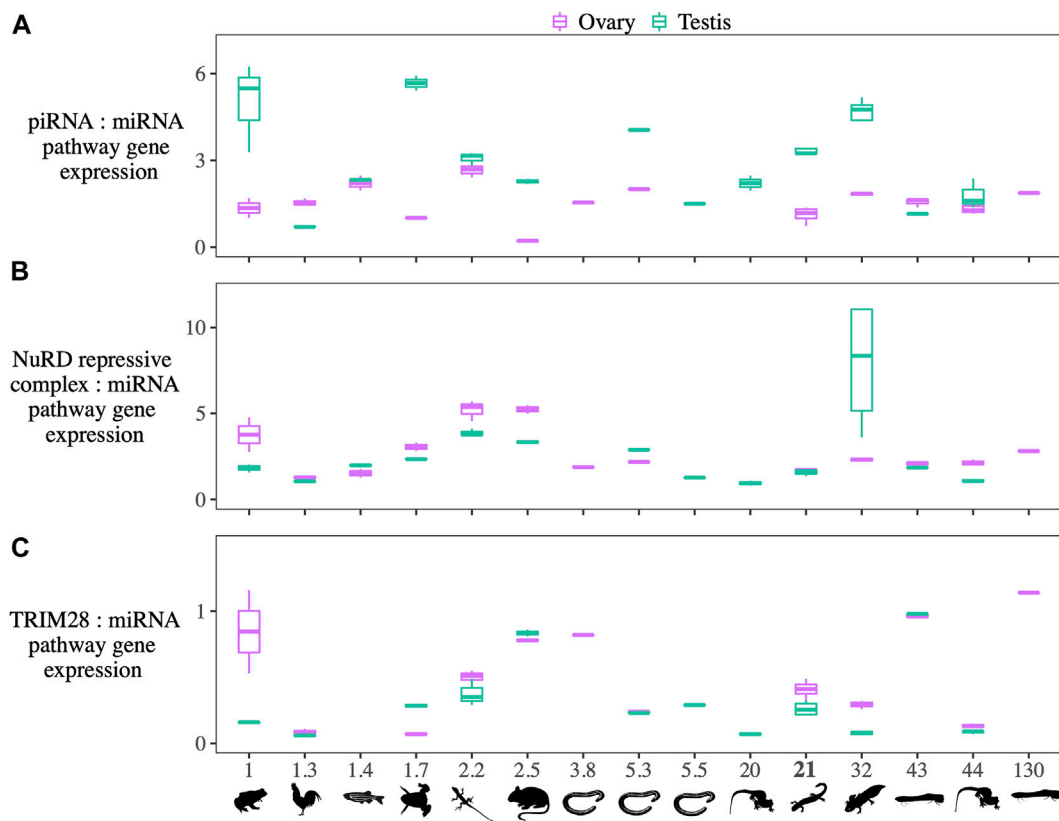


FIGURE 5

(A) The ratio of the summed expression of piRNA pathway genes, (B) NuRD and associated repressive complex genes, and (C) TRIM28 to the summed expression of miRNA pathway genes in species with diverse genome sizes. The species and their genome sizes (Gb) from left to right are: *Platyplectrum ornatum* (1), *Gallus gallus* (1.3), *Danio rerio* (1.4), *Xenopus tropicalis* (1.7), *Anolis carolinensis* (2.2), *Mus musculus* (2.5), *Geotrypetes seraphini* (3.8), *Rhinatrema bivittatum* (5.3), *Caecilia tentaculate* (5.5), *Pleurodeles waltl* (20), *Ranodon sibiricus* (21), *Ambystoma mexicanum* (32), *Protopterus annectens* (43), *Cynops orientalis* (44), and *Protopterus aethiopicus* (~130).

2.6 Gonadal expression of TE silencing machinery does not correlate with genome size in either sex

Across the range of genome sizes from 1 to 130 Gb, we find no correlations between genome size and 1) the expression of piRNA processing genes, 2) NuRD complex and associated genes establishing a repressive transcriptional environment, or 3) TRIM28. Interestingly, five of the six highest piRNA pathway expression levels are found in amphibians, the clade with the most variation in genome size (Figure 5, Supplementary File S9).

3 Discussion

3.1 Permissive TE environment despite comprehensive piRNA-mediated silencing

The transposable element community in *R. sibiricus* is comparable in diversity to other gigantic amphibian genomes and shares many of the same abundant TE superfamilies (e.g., LTR/Gypsy, DIRS/DIRS and LINE/L1) (Sun et al., 2012; Sun and Mueller, 2014; Wang et al., 2021a). However, *R. sibiricus* differs from

other salamanders in having high levels of LINE/Jockey, a superfamily shown to be abundant in the caecilian *Ichthyophis bannanicus*, but rare in other salamanders (Wang et al., 2021a). Both genomic and transcriptomic data suggest that all TE superfamilies are potentially experiencing ongoing transposition in *R. sibiricus*. Thus, like other gigantic amphibian genomes, *R. sibiricus* appears to have attained its large size because of the expansion of multiple types of TEs, supporting the notion of amphibian genomes as permissive TE environments. Low deletion rates can mean persistence of TEs until mutation accumulation renders them unrecognizable based on sequence similarity; thus, somewhat surprisingly, larger amphibian genomes are not always identified as having larger TE contents (Frahry et al., 2015; Keinath et al., 2015; Novák et al., 2020; Haley and Mueller, 2022). Overall relative TE expression levels in *R. sibiricus* are comparable to those seen in the gonads of vertebrates with typical genome sizes (Pasquesi et al., 2020). In addition, all of the putatively active TE superfamilies are targeted by piRNAs, and piRNA levels are correlated with TE expression at the superfamily level, consistent with patterns in *Drosophila* and suggesting that the scope, if not efficacy, of TE silencing in *R. sibiricus* is comparable to other species (Kelleher and Barbash, 2013; Saint-Leandre et al., 2020).

3.2 Sex-biased TE expression and silencing

Transposable element expression is higher in *R. sibiricus* testes than ovaries, a pattern also reported in *Drosophila* (Wei et al., 2022) and the medaka fish *O. latipes* (Saint-Leandre et al., 2020; Dechaud et al., 2021), but opposite the pattern reported in the carrion crow *Corvus corone* (Warmuth et al., 2022) and different from the non-sex-biased TE expression in the newt *C. orientalis* (Carducci et al., 2021). In *Drosophila*, testes expression levels of TE-mapping piRNAs and piRNA pathway genes, as well as the ping-pong signature, are lower than ovary expression levels, suggesting that lower male piRNA-mediated silencing contributes to higher male TE expression (Saint-Leandre et al., 2020; Chen et al., 2021). In *O. latipes*, on the other hand, testes expression levels of TE-mapping piRNAs are higher than ovary expression levels—a pattern also observed in zebrafish—suggesting that higher male piRNA-mediated silencing may actually be correlated with high male TE expression in these two fish species (Houwing et al., 2007; Kneitz et al., 2016). In *R. sibiricus*, TE-mapping piRNA counts are similar between the gonads of the two sexes, despite higher relative expression of putative piRNAs in testes than ovaries (Figures 3A,B). However, the ping-pong amplification signature is higher in ovaries, as is the number of piRNAs per expressed TE transcript, suggestive of a more robust piRNA-directed silencing response in females (Figure 3C; Figure 4A). On the other hand, the piRNA pathway protein expression levels are higher in testes, and ping-pong piRNA counts are higher in testes, suggesting the opposite case of a more robust response in males (Figure 4B; Figure 5).

Sex-specific differences in gonadal TE expression have also been explained by factors other than variation in TE silencing; for example, in systems with heteromorphic sex chromosomes, sex-biased TE expression has been attributed to different TE dynamics on the sex-limited chromosome (Y in XY systems, or W in ZW systems). TE abundance is higher on sex-limited chromosomes because of lower effective population size, lack of recombination, and lower gene density. In addition, TE expression per locus has been shown to be higher on the sex-limited chromosome itself—as well as genome-wide—in the heterogametic sex in *Drosophila* (Y, males) and in crows (*C. corone*; W, females) (Wei et al., 2020; Warmuth et al., 2022). The mechanism for higher TE expression in the heterogametic sex in these cases remains incompletely understood, but may involve TEs affecting their own genome-wide regulation *in trans* or the heightened conflict between creating a repressive chromatin state to silence TEs while maintaining open chromatin to allow genic transcription on a degenerating chromosome (Wei et al., 2020; Warmuth et al., 2022). Neither *R. sibiricus* nor *O. latipes* has heteromorphic sex chromosomes (Hillis and Green, 1990; Matsuda et al., 2002; Evans et al., 2012; Perkins et al., 2019), yet both show sex-biased TE expression, and only *Oryzias* shows unambiguous sex-biased TE-targeting piRNA expression; taken together, these data reveal that the difference in TE expression between sexes reflects different underlying causes across species. The relationships among sex-biased TE expression, sex determination, and TE silencing are an important target for future research, but irrespective of the

underlying mechanisms, the sex with higher TE activity contributes more to the species' genomic TE load (Wei et al., 2020). In *R. sibiricus*, that sex is the male, provided that TE expression is a reasonable proxy for transposition.

3.3 The TE-silencing arms race dynamic across genome sizes

Transposable elements and the silencing machinery of their hosts are engaged in an arms race in which a novel TE family initially proliferates, the host evolves silencing based on TE sequence identification, and the TE subsequently diverges to evade silencing—or that particular TE remains permanently silenced, but a novel TE invades the host genome and begins the cycle anew (Luo et al., 2020; Zhang et al., 2020; Said et al., 2022; Wei et al., 2022). If balanced by deletion of TE sequences, this arms-race dynamic can be associated with fairly stable genome size over evolutionary timescales, despite turnover in TE content (Kapusta et al., 2017). To yield an overall evolutionary trend in genome size, the long-term balance between TE insertion and deletion has to become skewed in favor of one or the other, with deletion bias leading to genome contraction and insertion bias leading to genome expansion (Nam and Ellegren, 2012).

It has been suggested in the literature that large genomes may be manifestations of an arms race between TEs and the silencing of their hosts, but that this arms race involves the TE community as a whole rather than individual TE families—and the species with the gigantic genome has been interpreted as both the current “attacker” and “defender” in the arms race. For example, Meyer et al. (2021) suggested that TE silencing machinery did not adapt to reduce TE expansion in the Australian lungfish, based on high genomic TE abundance and ongoing TE expression. In the strawberry poison dart frog, which has a moderately expanded genome size of 6.76 Gb, a widespread failure to silence TEs was suggested based on high genomic TE abundance, germline TE expression of diverse TEs, and the presence of an identified *piwi* transcript in only two of five individuals sampled (Rogers et al., 2018). In the salamander *D. fuscus*, less comprehensive piRNA pathway-mediated TE silencing was suggested based on a relatively low percentage of TE-mapping piRNAs (Madison-Villar et al., 2016). In all three of these examples, the TEs are suggested to be currently on the attack. On the other hand, in the African lungfish, Wang et al. (2021b) suggested that the KRAB-ZFP TE transcriptional silencing machinery has expanded in scope in response to the high genomic TE load. Similarly, in the newt *C. orientalis*, it was suggested that TE silencing is now enhanced in response to high TE load, which accumulated in the past during a period of increased TE mobilization (Carducci et al., 2021). In both of these examples, the TEs are suggested to be currently on the defensive. Thus, two opposite predictions for TE silencing in gigantic genomes—either increased or decreased—have been proposed to be met in different extant organisms, albeit with datasets that are not necessarily comparable. This apparent conflict can be resolved by considering that the attack/defense status of TEs and their silencing reflect where the lineage currently exists in the dynamic cycle between TE and host dominance. Our results revealing no consistent pattern in TE

silencing pathway expression levels and genome size (Figure 5) are consistent with this interpretation. At large sizes, it is not the size of the genome itself that likely predicts the efficacy of the TE silencing machinery, but more likely the directional trend in genome size evolution; genomes that are contracting are more likely to have effective TE silencing, whereas genomes undergoing expansion are more likely to have reduced TE silencing. In the absence of comparable data (including small RNA, TE expression and amplification, and silencing pathway expression) for other species with known trends in genome size evolution, we opt for a conservative position and do not infer *R. sibiricus*' current position in the TE/host dynamic arms race cycle.

The mechanisms by which global TE silencing mechanisms can be subverted by a community of TEs, and then evolve to regain stricter control, are not yet well-understood. A few studies in invertebrates have begun to reveal differences in TE and silencing dynamics in genomes of different sizes. In a pairwise comparison of grasshopper species with different genome sizes, Liu et al. revealed that the species with the larger genome had higher TE expression, lower piRNA abundance, and lower expression of the piRNA biogenesis gene *HENMT*, which suggested that lower piRNA-mediated TE silencing was permissive to higher TE activity and genome expansion (Liu et al., 2022). A comparison between *Drosophila melanogaster* and the mosquito *Aedes aegypti*, which has a larger genome (1.38 Gb versus 180 Mb), revealed that the mosquito has a higher TE load and a smaller percentage of TE-mapping piRNAs (Arensburger et al., 2011). Future studies that leverage the large range of genome sizes present in vertebrates, emphasizing comprehensive across-species data on TE activity and TE silencing in a phylogenetic context to allow ancestral genome size reconstruction, will continue to shed light on how TEs and their hosts coevolve to achieve gigantic genomes.

4 Materials and methods

4.1 Specimen information

We collected three male adult *R. sibiricus* from the wild of Wenquan County, Xinjiang Uygur Autonomous Region of China, and egg-hatched and raised one male and four females in an aquarium of Xinjiang Normal University from eggs originally collected from the same field site as the wild males. All these individuals were collected during the breeding season of August 2017, and all adults had a snout-tail length of 16–21 cm and a body mass of 12–35 g prior to euthanasia (Supplementary Files S1). Wild-caught adults were euthanized upon return to the laboratory and were not kept alive in captivity. Collection, hatching, and euthanasia were performed following Animal Care and Use Protocols approved by Chengdu Institute of Biology, Chinese Academy of Sciences.

4.2 Genome size estimation

Blood smears were prepared from a formalin-fixed specimen of *R. sibiricus* collected from the Borokhudzir River Valley in the Junggar Alatau mountains in Kazakhstan and nuclear area was measured from Fuelgen-stained red blood cell nuclei using the ImagePro® image analysis program (Itgen et al., 2022). Blood smears of the reference

standards *A. mexicanum* (32 Gb; Nowoshilow et al., 2018) and the Iberian ribbed newt *Pleurodeles waltl* (20 Gb; Gregory, 2022) were prepared and analyzed at the same time under the same conditions.

4.3 Genomic shotgun library creation, sequencing, and assembly

Total DNA was extracted from muscle tissue using the modified low-salt CTAB extraction of high-quality DNA procedure (Arseneau et al., 2017). DNA quality and concentration were assessed using agarose gel electrophoresis and a NanoDrop Spectrophotometer (ThermoFisher Scientific, Waltham, MA), and a PCR-free library was prepared using the NEBNext Ultra DNA Library Prep Kit for Illumina. Sequencing was performed on one lane of a HiSeq 2,500 platform (PE250). Library preparation and sequencing were performed by the Beijing Novogene Bioinformatics Technology Co. Ltd. Raw reads were quality-filtered and adapter-trimmed using Trimmomatic-0.39 (Bolger et al., 2014) with default parameters. In total, the genomic shotgun dataset included 11,960,858 reads. After filtering and trimming, 11,168,678 reads covering a total length of 2,314,096,923 bp remained. Thus, the sequencing coverage is about 10.9% (0.1X coverage). Filtered, trimmed reads were assembled into contigs using dipSPAdes 3.12.0 (Bankevich et al., 2012) with default parameters, yielding 478,991 contigs with an N50 of 447 bp and a total length of 249,425,929 bp. This is comparable to our assembly of low-coverage sequencing reads of another gigantic amphibian genome (*I. bannanicus*, 12.2 Gb; 130,417 contigs with an N50 of 740 bp and a total length of 1,560,938,851 bp) (Wang et al., 2021a), albeit on the low side for complete genome assemblies (Ellis et al., 2021). For the purposes of this study, the assembly was used to create contigs representing TE superfamilies to which we could map genomic reads; this only requires contigs that span the length of TEs (on the order of kilobases).

4.4 Mining and classification of repeat elements

The PiRATE pipeline was used as in the original publication (Berthelier et al., 2018), including the following steps: 1) Contigs representing repetitive sequences were identified from the assembled contigs using similarity-based, structure-based, and repetitiveness-based approaches. The similarity-based detection programs included RepeatMasker v-4.1.0 (<http://repeatmasker.org/RepeatMasker/>), using Repbase20.05_REPET.embl.tar.gz as the library instead) and TE-HMMER (Eddy, 2011). The structural-based detection programs included LTRharvest (Ellinghaus et al., 2008), MGEscan non-LTR (Rho and Tang, 2009), HelSearch (Yang et al., 2009), MITE-Hunter (Han and Wessler, 2010), and SINEfinder (Wenke et al., 2011). The repetitiveness-based detection programs included TEde novo (Flutre et al., 2011) and RepeatScout (Price et al., 2005). 2) Repeat consensus sequences (e.g., representing multiple subfamilies within a TE family) were also identified from the cleaned, filtered, and unassembled reads with dnaPipeTE (Goubert et al., 2015) and RepeatModeler (<http://www.repeatmasker.org/RepeatModeler/>). 3) Contigs identified by each individual program in steps 1 and 2, above, were filtered to remove those <100 bp in length and clustered with CD-HIT-est (Li and Godzik,

2006) to reduce redundancy (100% sequence identity cutoff). This yielded a total of 155,999 contigs. 4) All 155,999 contigs were then clustered together with CD-HIT-est (100% sequence identity cutoff), retaining the longest contig and recording the program that classified it. 46,090 contigs were filtered out at this step. 5) The remaining 109,909 repeat contigs were annotated as TEs to the levels of order and superfamily in Wicker's hierarchical classification system (Wicker et al., 2007), modified to include several recently discovered TE superfamilies using PASTEC (Hoede et al., 2014), and checked manually to filter chimeric contigs and those annotated with conflicting evidence (Supplementary File S2). 6) All classified repeats ("known TEs" hereafter), along with the unclassified repeats ("unknown repeats" hereafter) and putative multi-copy host genes, were combined to produce a *Ranodon*-derived repeat library. 7) For each superfamily, we collapsed the contigs to 95% and 80% sequence identity using CD-HIT-est to provide an overall view of within-superfamily diversity; 80% is the sequence identity threshold used to define TE families (Wicker et al., 2007).

4.5 Characterization of the overall repeat element landscape

Overlapping paired-end shotgun reads were merged using PEAR v.0.9.11 (Zhang et al., 2014) with the following parameter values based on our library insert size and trimming parameters: min-assemble-length 36, max-assemble-length 490, min-overlap size 10. After merging, 7,385,166 reads remained (including both merged and singletons), with an N50 of 388 bp and total length of 1,997,175,501 bp. To calculate the percentage of the *R. sibiricus* genome composed of different TEs, these shotgun reads were masked with RepeatMasker v-4.1.0 using two versions of our *Ranodon*-derived repeat library: one that included the unknown repeats and the other that excluded them. In both cases, simple repeats were identified using the Tandem Repeat Finder module implemented in RepeatMasker. The overall results were summarized at the levels of TE class, order, and superfamily.

4.6 Measuring diversity of the genomic TE community

Unknown repeats were excluded from the analysis, as were TEs that could only be annotated down to the level of Class. Simpson's diversity index is expressed as the variable D , calculated by: $D = \frac{\sum_{i=1}^{n(n-1)}}{N(N-1)}$ (Simpson, 1949). D is the probability that two individuals at random pulled from a community will be from the same species. We report $1-D$, or the Gini-Simpson's index, which is more intuitive. The Shannon's diversity index H is calculated by: $H = -\sum_{i=1}^s p_i \ln p_i$ (Shannon, 1948). The higher the value of H , the greater the diversity.

4.7 Amplification history of TE superfamilies

To summarize the overall amplification history of TE superfamilies and test for ongoing activity, the perl script parseRM.pl (Kapusta et al., 2017) was used to parse the raw output files from RepeatMasker (.align) and report the sequence divergence between each read and its respective consensus sequence

(parameter values = -1 50,1 and -a 5). The repeat library used to mask the reads comprised the 55,327 TE contigs classified by the PiRATE pipeline and clustered at 100% sequence identity. Each TE superfamily is therefore represented by multiple consensus sequences corresponding to the family and subfamily TE taxonomic levels (*i.e.*, not the distant common ancestor of the entire superfamily). For each superfamily, histograms were plotted to summarize the percent divergence of all reads from their closest (*i.e.*, least divergent) consensus sequence. These histograms do not allow the delineation between different amplification dynamics scenarios (*i.e.*, a single family with continuous activity versus multiple families with successive bursts of activity). Rather, these global overviews were examined for overall shapes consistent with ongoing activity (*i.e.*, the presence of TE loci <1% diverged from the ancestral sequence and a unimodal, right-skewed, J-shaped, or monotonically decreasing distribution).

4.8 Transcriptome library creation, sequencing, assembly, and TE annotation

Total RNA was extracted separately from testis ($n = 4$) and ovary ($n = 4$) tissues using TRIzol (Invitrogen). For each sample, RNA quality and concentration were assessed using agarose gel electrophoresis, a NanoPhotometer spectrophotometer (Implen, CA), a Qubit 2.0 Fluorometer (ThermoFisher Scientific), and an Agilent BioAnalyzer 2,100 system (Agilent Technologies, CA), requiring an RNA integrity number (RIN) of 8.5 or higher; one ovary sample failed to meet these quality standards and was excluded from downstream analyses. Sequencing libraries were generated using the NEBNext Ultra RNA Library Prep Kit for Illumina following the manufacturer's protocol. After cluster generation of the index-coded samples, the library was sequenced on one lane of an Illumina HiSeq 4,000 platform (PE 150). Transcriptome sequences were filtered using Trimmomatic-0.39 with default parameters (Bolger et al., 2014). 30, 848, 170 to 39, 695, 323 reads were retained for each testis or ovary sample, and in total, 290, 925, 984 reads remained, with a total length of 42, 385, 060,050 bp. Remaining reads of all testis and ovary samples were combined and assembled using Trinity 2.12.0 (Haas et al., 2013), yielding 573,144 contigs (*i.e.*, putative assembled transcripts). Contigs were clustered using CD-hit-est (95% identity). Completeness of this final *de novo* transcriptome assembly were assessed using the BUSCO pipeline (Simao et al., 2015).

Expression levels of contigs in each sample were measured with Salmon (Patro et al., 2017), and contigs with no raw counts were removed. To annotate the remaining contigs containing autonomous TEs, BLASTp and BLASTx were used against Repbase with an E-value cutoff of $1E-5$ and $1E-10$, respectively. The aligned length coverage was set to exceed 80% of the queried transcriptome contigs. To annotate contigs containing non-autonomous TEs, RepeatMasker was used with our *Ranodon*-derived genomic repeat library of non-autonomous TEs (LARD-, TRIM-, MITE-, and SINE-annotated contigs) and the requirement that the transcriptome/genomic contig overlap was >80 bp long, >80% identical in sequence, and covered >80% of the length of the genomic contig. Contigs annotated as conflicting autonomous and non-autonomous TEs were filtered out.

To identify contigs that contained endogenous *R. sibiricus* genes, the Trinotate annotation suite (Bryant et al., 2017) was used with an E-value cutoff of $1E-5$ for both BLASTx and BLASTp against the Uniport database, and $1E-5$ for HMMER against the Pfam database (Wheeler and Eddy, 2013). To identify contigs that contained both a TE and an endogenous gene (i.e., putative cases where a TE and a gene were co-transcribed on a single transcript), all contigs that were annotated both by Repbase and Trinotate were examined, and the ones annotated by Trinotate to contain a TE-encoded protein (i.e., the contigs where Repbase and Trinotate annotations were in agreement) were not further considered. The remaining contigs annotated by Trinotate to contain a non-TE gene (i.e., an endogenous *Ranodon* gene) and also annotated either by Repbase to include a TE-encoded protein or by blastn to include a non-autonomous TE were filtered out for the expression analysis.

4.9 Gonadal TE expression quantification in males and females

Expression levels of the individual TE superfamilies were calculated by averaging the TPM values among replicates of each sex and then summing the average TPM of all contigs annotated to each superfamily. For TE superfamilies detected in both the genomic and transcriptomic datasets, we tested for a relationship between genomic abundance and expression levels in the gonads of each sex using linear regression on log-transformed data.

To identify differentially expressed contigs between testes and ovaries, DESeq2 (Love et al., 2014) was used with an adjusted *p*-value cut off of 0.05. Among the 15,011 total differentially expressed transcripts between testes and ovaries (including TEs, endogenous genes, and unannotated contigs), 869 were TEs, representing 18 superfamilies and other unknown TEs. Superfamilies with fewer than 10 differentially expressed transcripts between testes and ovaries were removed, leaving nine superfamilies; for each, we tested for a difference in expression between testes and ovaries using a *t*-test.

4.10 Identification of putative piRNAs from small RNA-seq data

Small RNA libraries were prepared for each sample using the NEBNext® Multiplex Small RNA Library Prep Set for Illumina® (NEB, United States) following the manufacturer's recommendations, and index codes were added to attribute sequences to each sample. Briefly, the NEB 3' SR Adaptor (5'-AGATCGGAAGAGCACACGTCT-3') was ligated to the 3' end of small RNA molecules. After the 3' ligation reaction, the SR RT Primer was hybridized to the excess 3' SR Adaptor (that remained free after the 3' ligation reaction), transforming the single-stranded DNA adaptor into a double-stranded DNA molecule (dsDNAs). This step was important for preventing adaptor-dimer formation, and because dsDNAs are not substrates for ligation mediated by T4 RNA Ligase 1, they therefore would not ligate to the 5' SR Adaptor (5'-GTTTCAGAGTTCTACAGTCCGACGATC-3') in the subsequent ligation step. The 5' end adapter was then ligated to the 5' ends of small RNA molecules. First strand cDNA was

synthesized using M-MuLV Reverse Transcriptase (Rnase H). PCR amplification was performed using LongAmp Taq 2X Master Mix, SR Primer for Illumina, and index primers. PCR products were purified on an 8% polyacrylamide gel (100V, 80 min). DNA fragments corresponding to ~140–160 bp (the length of a small non-coding RNA plus the 3' and 5' adaptors) were recovered and dissolved in 8 μ L elution buffer. Library quality was assessed on the Agilent Bioanalyzer 2,100 using DNA High Sensitivity Chips. Clustering of index-coded samples was performed on a cBot Cluster Generation System using the TruSeq SR Cluster Kit v3-cBot-HS (Illumina) according to the manufacturer's instructions. After cluster generation, libraries were sequenced on an Illumina HiSeq 2,500 platform (SE50).

We filtered low-quality sequences using the fastq_quality_filter (-q 20, -p 90) in the FASTX-Toolkit v0.0.13 (http://hannonlab.cshl.edu/fastx_toolkit/). We removed the adapter sequence with a minimum overlap of 10 bp from the 3'-end, discarded untrimmed reads, and selected those with a minimum length of 18 bp and a maximum length of 40 bp (after cutting adapters) and no Ns using cutadapt v2.8 (Martin, 2011). Reads mapping to the mitochondrial genome (NCBI code: AJ419960) and riboRNAs (NCBI codes: DQ283664, AJ279506, MH806872) were identified and filtered out using Bowtie v1.1.0 (Langmead et al., 2009). Overall, more reads were filtered out based on length and rRNA identity in ovaries than testes (Supplementary File S5). miRNAs 21–24 nt in length were annotated using Bowtie v1.1.0 to identify hits to miRbase 22.1 (Kozomara et al., 2019) in each testis and ovary.

To test for the predicted bias towards U at the first 5' nucleotide position of piRNAs, we calculated the proportion of small RNAs with each nucleotide in the first position. Based on this result, and the overall length distribution of RNAs between 18 and 40 nt, we conservatively defined putative piRNAs as those ranging from 25–30 nt, and we selected these using the seqkit software (Shen et al., 2016). We mapped these putative piRNAs to our transcriptome assembly using Bowtie and identified piRNAs that map to autonomous TEs (i.e., those that include transposition-related ORFs) in the sense and antisense orientations.

4.11 Ping-pong signature analysis

Secondary piRNA biogenesis associated with piRNA-targeted post-transcriptional TE silencing produces a distinctive “ping-pong signature” in the piRNA pool, which consists of a 10 bp overlap between the 5' ends of antisense and sense piRNAs. The ping-pong signature for each individual was analyzed using the following approach: First, TE transcripts that were not mapped by both sense-oriented and antisense-oriented piRNAs were filtered out using Bowtie, allowing 0 mismatches for sense mapping under the assumption that piRNAs derived directly from an RNA target should have the identical sequence (Teefy et al., 2020) and three mismatches for antisense mapping because cleavage of RNA targets can occur with imperfect base-pairing (Zhang et al., 2015). Second, the fractions of overlapping pairs of sense/antisense piRNAs corresponding to specific lengths, as well as the Z-score measuring the significance of each ping-pong signature, were generated using the 1_piRNA_and_Degradome_Counts.Rmd and 3_Ping_Pong_Phasing.Rmd scripts (Teefy et al., 2020).

4.12 Putative piRNAs targeting TE superfamilies

To estimate levels of piRNAs targeting each TE superfamily, putative piRNAs were mapped to the TE transcripts using the ‘align_and_estimate_abundance.pl’ script of Trinity (Haas et al., 2013). Reads per million (RPM) values were calculated for each TE contig and then averaged across individuals of each sex. For each sex, overall putative piRNA levels targeting each TE superfamily were calculated by summing across all contigs annotated to the same TE superfamily. We tested for a correlation between TE superfamily expression level and targeting piRNA abundance using linear regression on the log-transformed variables. Ping-pong piRNAs mapping to TE superfamilies were also counted and tested for a correlation with TE superfamily expression levels using linear regression.

4.13 Germline TE silencing pathway expression across genome sizes

To test for an association between overall piRNA or KRAB-ZFP pathway activity and genome size, we first compiled male and female gonad RNA-Seq datasets for vertebrates of diverse genome sizes, including *P. ornatum* (ornate burrowing frog), *Gallus gallus* (chicken), *D. rerio* (zebrafish), *Xenopus tropicalis* (Western clawed frog), *A. carolinensis* (green anole), *Mus musculus* (mouse), *Geotrypetes seraphini* (Gaboon caecilian), *Rhinatrema bivittatum* (two-lined caecilian), and *Caecilia tentaculata* (bearded caecilian) spanning genome sizes from 1.0–5.5 Gb, and *P. waltil* (the Iberian ribbed newt), *A. mexicanum* (the Mexican axolotl), *C. orientalis* (the fire-bellied newt), *P. annectens*, and *P. aethiopicus* (African and marbled lungfishes) spanning genome sizes from 20–~130 Gb (Supplementary Files S8,S9). We performed *de novo* assemblies using the same pipeline as for *R. sibiricus* on all obtained datasets.

We identified transcripts of 21 genes receiving a direct annotation of piRNA processing in vertebrates in the Gene Ontology knowledgebase that were present in the majority of our target species: ASZ1, BTBD18 (BTBD1), DDX4, EXD1, FKBP6, GPAT2, HENMT1 (HENMT), MAEL, MOV10I1 (M10L1), PIWIL1, PIWIL2, PIWIL4, PLD6, TDRD1, TDRD5, TDRD6, TDRD7, TDRD9, TDRD12 (TDR12), TDRD15 (TDR15), and TDRKH. In addition, we identified transcripts of 14 genes encoding proteins that create a transcriptionally repressive chromatin environment in response to recruitment by PIWI proteins or KRAB-ZFP proteins, 12 of which received a direct annotation of NuRD complex in the Gene Ontology knowledgebase and 2 of which were taken from the literature: CBX5, CHD3, CHD4, CSNK2A1 (CSK21), DNMT1, GATAD2A (P66A), MBD3, MTA1, MTA2, RBBP4, RBBP7, SALL1, SETDB1 (SETB1), and ZBTB7A (ZBT7A) (Ecco et al., 2017; Wang et al., 2023). Finally, we identified TRIM28, which bridges this repressive complex to TE-bound KRAB-ZFP proteins in tetrapods, lungfishes, and coelacanths (Ecco et al., 2017). For comparison, we identified transcripts of 14 protein-coding genes receiving a direct annotation of miRNA processing in vertebrates in the Gene Ontology

knowledgebase, which we did not predict to differ in expression based on genome size: ADAR (DSRAD), AGO1, AGO2, AGO3, AGO4, DICER1, NUP155 (NU155), PUM1, PUM2, SNIP1, SPOUT1 (CI114), TARBP2 (TRBP2), TRIM71 (LIN41), and ZC3H7B. Expression levels for each transcript in each individual were measured with Salmon (Patro et al., 2017) (Supplementary File S10).

As a proxy for overall piRNA silencing activity, for each individual, we calculated the ratio of total piRNA pathway expression (summed TPM of 21 genes) to total miRNA pathway expression (summed TPM of 14 genes). As a proxy for transcriptional repression driven by both the piRNA pathway and KRAB-ZFP binding activity, we calculated the ratio of total transcriptional repression machinery expression (summed TPM of 14 genes) to total miRNA pathway expression. Finally, we calculated the ratio of TRIM28 expression to total miRNA pathway expression for each individual. We also calculated these ratios with a more conservative dataset allowing for no missing genes; this yielded 15 piRNA pathway genes, 9 KRAB-ZFP genes, and 13 miRNA genes. We plotted these ratios to reveal any relationship between TE silencing pathway expression and genome size.

Data availability statement

The data presented in the study are deposited in the Genome Sequence Archive repository <http://bigd.big.ac.cn/gsa>, accession numbers CRA008892, CRA008899, CRA008900.

Ethics statement

The animal study was reviewed and approved by Chengdu Institute of Biology, Chinese Academy of Sciences.

Author contributions

JW: Conceptualization, Methodology, Software, Formal analysis, Investigation, Resources, Data curation, Writing–original draft, Writing–review and editing, Visualization, Funding acquisition. LY: Specimen collection. JT, JL, CS, MI, and GC: Methodology, Software. SS: Investigation, Resources. GZ: Methodology, Formal analysis, Writing–original draft, Writing–review and editing, Visualization. RM: Conceptualization, Formal analysis, Investigation, Resources, Writing–original draft, Writing–review and editing, Supervision, Project administration, Funding acquisition. All authors read and approved the final manuscript.

Funding

This work was supported by the National Natural Science Foundation of China (Grant Nos. 32170435, 31570391 to JW) and the National Science Foundation of United States (Grant No. 1911585 to RM).

Acknowledgments

We gratefully acknowledge Ye Xu and Yuzhou Gong for target tissue dissection; Xiuling Wang for help in field work; Nikolay Poyarkov and Koji Iizuka for blood slides; and Jianping Jiang, Ava Louise Haley, and Chaochao Yan for their expertise in facilitating data analysis.

Conflict of interest

The authors declare that the research was conducted in the absence of any commercial or financial relationships that could be construed as a potential conflict of interest.

References

- Almeida, M. V., Vernaz, G., Putman, A. L. K., and Miska, E. A. (2022). Taming transposable elements in vertebrates: From epigenetic silencing to domestication. *Trends Genet.* 38, 529–553. doi:10.1016/j.tig.2022.02.009
- AmphibiaWeb (2022). *AmphibiaWeb: Information on amphibian biology and conservation*. Berkeley, California: AmphibiaWeb.
- Aravin, A. A., Sachidanandam, R., Bourc'his, D., Schaefer, C., Pezic, D., Toth, K. F., et al. (2008). A piRNA pathway primed by individual transposons is linked to de novo DNA methylation in mice. *Mol. Cell* 31, 785–799. doi:10.1016/j.molcel.2008.09.003
- Aravin, A., Gaidatzis, D., Pfeffer, S., Lagos-Quintana, M., Landgraf, P., Iovino, N., et al. (2006). A novel class of small RNAs bind to MILI protein in mouse testes. *Nature* 442, 203–207. doi:10.1038/nature04916
- Arensburger, P., Hice, R. H., Wright, J. A., Craig, N. L., and Atkinson, P. W. (2011). The mosquito *Aedes aegypti* has a large genome size and high transposable element load but contains a low proportion of transposon-specific piRNAs. *BMC Genomics* 12, 606. doi:10.1186/1471-2164-12-606
- Arkhipova, I. R. (2018). Neutral theory, transposable elements, and eukaryotic genome evolution. *Mol. Biol. Evol.* 35, 1332–1337. doi:10.1093/molbev/msy083
- Arseneau, J. R., Steeves, R., and Laflamme, M. (2017). Modified low-salt CTAB extraction of high-quality DNA from contaminant-rich tissues. *Mol. Ecol. Resour.* 17, 686–693. doi:10.1111/1755-0998.12616
- Bankevich, A., Nurk, S., Antipov, D., Gurevich, A. A., Dvorkin, M., Kulikov, A. S., et al. (2012). SPAdes: A new genome assembly algorithm and its applications to single-cell sequencing. *J. Comput. Biol.* 19, 455–477. doi:10.1089/cmb.2012.0021
- Berthelier, J., Casse, N., Daccord, N., Jamilloux, V., Saint-Jean, B., and Carrier, G. (2018). A transposable element annotation pipeline and expression analysis reveal potentially active elements in the microalga *Tisochrysis lutea*. *BMC Genomics* 19, 378. doi:10.1186/s12864-018-4763-1
- Biscotti, M. A., Canapa, A., Forconi, M., Gerdol, M., Pallavicini, A., Scharl, M., et al. (2017). The small noncoding RNA processing machinery of two living fossil species, lungfish and coelacanth, gives new insights into the evolution of the Argonaute protein family. *Genome Biol. Evol.* 9, 438–453. doi:10.1093/gbe/evx017
- Bolger, A. M., Lohse, M., and Usadel, B. (2014). Trimmomatic: A flexible trimmer for Illumina sequence data. *Bioinformatics* 30, 2114–2120. doi:10.1093/bioinformatics/btu170
- Bourque, G., Burns, K. H., Gehring, M., Gorbunova, V., Seluanov, A., Hammell, M., et al. (2018). Ten things you should know about transposable elements. *Genome Biol.* 19, 199. doi:10.1186/s13059-018-1577-z
- Brennecke, J., Aravin, A. A., Stark, A., Dus, M., Kellis, M., Sachidanandam, R., et al. (2007). Discrete small RNA-generating loci as master regulators of transposon activity in *Drosophila*. *Cell* 128, 1089–1103. doi:10.1016/j.cell.2007.01.043
- Bryant, D. M., Johnson, K., Ditommaso, T., Tickle, T., Couger, M. B., Payzin-Dogru, D., et al. (2017). A tissue-mapped axolotl de novo transcriptome enables identification of limb regeneration factors. *Cell Rep.* 18, 762–776. doi:10.1016/j.celrep.2016.12.063
- Carducci, F., Carotti, E., Gerdol, M., Greco, S., Canapa, A., Barucca, M., et al. (2021). Investigation of the activity of transposable elements and genes involved in their silencing in the new *Cynops orientalis*, a species with a giant genome. *Sci. Rep.* 11, 14743. doi:10.1038/s41598-021-94193-6
- Castanera, R., Borgognone, A., Pisabarro, A. G., and Ramirez, L. (2017). Biology, dynamics, and applications of transposable elements in basidiomycete fungi. *App Microbiol. Biotech.* 101, 1337–1350. doi:10.1007/s00253-017-8097-8

Publisher's note

All claims expressed in this article are solely those of the authors and do not necessarily represent those of their affiliated organizations, or those of the publisher, the editors and the reviewers. Any product that may be evaluated in this article, or claim that may be made by its manufacturer, is not guaranteed or endorsed by the publisher.

Supplementary material

The Supplementary Material for this article can be found online at: <https://www.frontiersin.org/articles/10.3389/fcell.2023.1124374/full#supplementary-material>

- Castel, S. E., and Martienssen, R. A. (2013). RNA interference in the nucleus: Roles for small RNAs in transcription, epigenetics and beyond. *Nat. Rev. Genet.* 14, 100–112. doi:10.1038/nrg3355
- Chen, P., Kotov, A. A., Godneeva, B. K., Bazylev, S. S., Olenina, L. V., and Aravin, A. A. (2021). piRNA-mediated gene regulation and adaptation to sex-specific transposon expression in *D. melanogaster* male germline. *Genes and Dev.* 35, 914–935. doi:10.1101/gad.345041.120
- Czech, B., and Hannon, G. J. (2016). One loop to rule them all: The ping-pong cycle and piRNA-guided silencing. *Trends Biochem. Sci.* 41, 324–337. doi:10.1016/j.tibs.2015.12.008
- Czech, B., Munafò, M., Ciabrelli, F., Eastwood, E. L., Fabry, M. H., Kneuss, E., et al. (2018). piRNA-guided genome defense: from biogenesis to silencing. *Annu. Rev. Genet.* 52, 131–157. doi:10.1146/annurev-genet-120417-031441
- De Koning, A. J., Gu, W., Castoe, T. A., Batzer, M. A., and Pollock, D. D. (2011). Repetitive elements may comprise over two-thirds of the human genome. *PLoS Genet.* 7, e1002384. doi:10.1371/journal.pgen.1002384
- Dechaud, C., Miyake, S., Martinez-Bengochea, A., Scharl, M., Volff, J.-N., and Naville, M. (2021). Clustering of sex-biased genes and transposable elements in the genome of the medaka fish *Oryzias latipes*. *Genome Biol. Evol.* 13, evab230. doi:10.1093/gbe/evab230
- Deniz, Ö., Frost, J. M., and Branco, M. R. (2019). Regulation of transposable elements by DNA modifications. *Nat. Rev. Genet.* 20, 417–431. doi:10.1038/s41576-019-0106-6
- Doolittle, W. F., and Sapienza, C. (1980). Selfish genes, the phenotype paradigm and genome evolution: fish genes, the phenotype paradigm and genome evolution. *Nature* 284, 601–603. doi:10.1038/284601a0
- Ecco, G., Imbeault, M., and Trono, D. (2017). KRAB zinc finger proteins. *Development* 144, 2719–2729. doi:10.1242/dev.132605
- Eddy, S. R. (2011). Accelerated profile HMM searches. *PLoS Comput. Biol.* 7, e1002195. doi:10.1371/journal.pcbi.1002195
- Ellinghaus, D., Kurtz, S., and Willhoeft, U. (2008). LTRharvest, an efficient and flexible software for de novo detection of LTR retrotransposons. *BMC Bioinforma.* 9, 18. doi:10.1186/1471-2105-9-18
- Ellis, E. A., Storer, C. G., and Kawahara, A. Y. (2021). De novo genome assemblies of butterflies. *GigaScience* 10, giab041. doi:10.1093/gigascience/giab041
- Evans, B. J., Alexander Pyron, R., and Wiens, J. J. (2012). "Polyploidization and sex chromosome evolution in amphibians," in *Ployploidy and genome evolution* (Berlin, Germany: Springer), 385–410.
- Flutre, T., Duprat, E., Feuillet, C., and Quesneville, H. (2011). Considering transposable element diversification in de novo annotation approaches. *PLoS One* 6, e16526. doi:10.1371/journal.pone.0016526
- Frahry, M. B., Sun, C., Chong, R., and Mueller, R. L. (2015). Low levels of LTR retrotransposon deletion by ectopic recombination in the gigantic genomes of salamanders. *J. Mol. Evol.* 80, 120–129. doi:10.1007/s00239-014-9663-7
- Goubert, C., Modolo, L., Vieira, C., Valientemoro, C., Mavingui, P., and Boulesteix, M. (2015). De novo assembly and annotation of the Asian tiger mosquito (*Aedes albopictus*) repeatome with dnaPipeTE from raw genomic reads and comparative analysis with the yellow fever mosquito (*Aedes aegypti*). *Genome Biol. Evol.* 7, 1192–1205. doi:10.1093/gbe/evv050
- Gregory, T. R. (2022). Animal genome size database. Available at: <http://www.genomesize.com>.

- Gunawardane, L. S., Saito, K., Nishika, K. M., Kawamura, Y., Nagami, T., Siomi, H., et al. (2007). A slicer-mediated mechanism for repeat-associated siRNA 5' end formation in *Drosophila*. *Science* 315, 1587–1590. doi:10.1126/science.1140494
- Gutierrez, J., Platt, R., Opazo, J. C., Ray, D. A., Hoffmann, F., and Vandewege, M. (2021). Evolutionary history of the vertebrate Piwi gene family. *PeerJ* 9, e12451. doi:10.7717/peerj.12451
- Haas, B. J., Papanicolaou, A., Yassour, M., Grabherr, M., Blood, P. D., Bowden, J., et al. (2013). De novo transcript sequence reconstruction from RNA-seq using the Trinity platform for reference generation and analysis. *Nat. Protoc.* 8, 1494–1512. doi:10.1038/nprot.2013.084
- Haberer, G., Young, S., Bharti, A. K., Gundlach, H., Raymond, C., Fuks, G., et al. (2005). Structure and architecture of the maize genome. *Plant Physiol.* 139, 1612–1624. doi:10.1104/pp.105.068718
- Haley, A. L., and Mueller, R. L. (2022). Transposable element diversity remains high in gigantic genomes. *J. Mol. Evol.* 90, 332–341. doi:10.1007/s00239-022-10063-3
- Han, Y. J., and Wessler, S. R. (2010). MITE-hunter: A program for discovering miniature inverted-repeat transposable elements from genomic sequences. *Nucleic Acids Res.* 38, e199. doi:10.1093/nar/gkq862
- Hancks, D. C., and Kazazian, H. H. (2016). Roles for retrotransposon insertions in human disease. *Mob. DNA* 7, 9. doi:10.1186/s13100-016-0065-9
- Hillis, D. M., and Green, D. M. (1990). Evolutionary changes of heterogametic sex in the phylogenetic history of amphibians. *J. Evol. Biol.* 3, 49–64. doi:10.1046/j.1420-9101.1990.3010049.x
- Hoede, C., Arnoux, S., Moisset, M., Chaumier, T., Inizan, O., Jamilloux, V., et al. (2014). Paster: An automatic transposable element classification tool. *PLoS One* 9, e91929. doi:10.1371/journal.pone.0091929
- Hof, A. E., Campagne, P., Rigden, D. J., Yung, C. J., Lingley, J., Quail, M. A., et al. (2016). The industrial melanism mutation in British peppered moths is a transposable element. *Nature* 534, 102–105. doi:10.1038/nature17951
- Houwing, S., Kamminga, L. M., Berezikov, E., Cronembold, D., Girard, A., Van Den Elst, H., et al. (2007). A role for Piwi and piRNAs in germ cell maintenance and transposon silencing in Zebrafish. *Cell* 129, 69–82. doi:10.1016/j.cell.2007.03.026
- Imbeault, M., Helleboid, P.-Y., and Trono, D. (2017). KRAB zinc-finger proteins contribute to the evolution of gene regulatory networks. *Nature* 543, 550–554. doi:10.1038/nature21683
- Itgen, M. W., Siegel, D. S., Sessions, S. K., and Mueller, R. L. (2022). Genome size drives morphological evolution in organ-specific ways. *Evolution* 76 (7), 1453–1468. doi:10.1111/evo.14519
- Iwakawa, H.-O., and Tomari, Y. (2022). Life of RISC: Formation, action, and degradation of RNA-induced silencing complex. *Mol. Cell* 82, 30–43. doi:10.1016/j.molcel.2021.11.026
- Iwasaki, Y. W., Siomi, M. C., and Siomi, H. (2015). PIWI-interacting RNA: Its biogenesis and functions. *Annu. Rev. Biochem.* 84, 405–433. doi:10.1146/annurev-biochem-060614-034258
- Jiao, Y., Peluso, P., Shi, J., Liang, T., Stitzer, M. C., Wang, B., et al. (2017). Improved maize reference genome with single-molecule technologies. *Nature* 546, 524–527. doi:10.1038/nature22971
- Kapusta, A., Suh, A., and Feschotte, C. (2017). Dynamics of genome size evolution in birds and mammals. *Proc. Natl. Acad. Sci.* 114, E1460–E1469. doi:10.1073/pnas.1616702114
- Keinath, M. C., Timoshevskiy, V. A., Timoshevskaya, N. Y., Tsonis, P. A., Voss, S. R., and Smith, J. J. (2015). Initial characterization of the large genome of the salamander *Ambystoma mexicanum* using shotgun and laser capture chromosome sequencing. *Sci. Rep.* 5, 16413. doi:10.1038/srep16413
- Kelleher, E. S., and Barbash, D. A. (2013). Analysis of piRNA-mediated silencing of active TEs in *Drosophila melanogaster* suggests limits on the evolution of host genome defense. *Mol. Biol. Evol.* 30, 1816–1829. doi:10.1093/molbev/mst081
- Kneitz, S., Mishra, R. R., Chalopin, D., Postlethwait, J., Warren, W. C., Walter, R. B., et al. (2016). Germ cell and tumor associated piRNAs in the medaka and *Xiphophorus melanoma* models. *BMC Genomics* 17, 357. doi:10.1186/s12864-016-2697-z
- Kozomara, A., Birgaoanu, M., and Griffiths-Jones, S. (2019). miRBase: from microRNA sequences to function. *Nucleic Acids Res.* 47, D155–D162. doi:10.1093/nar/gky1141
- Lamichhaney, S., Catullo, R., Keogh, J. S., Clulow, S., Edwards, S. V., and Ezaz, T. (2021). A bird-like genome from a frog: Mechanisms of genome size reduction in the ornate burrowing frog, *Platyplectrum ornatum*. *Proc. Nat. Acad. Sci.* 118, e2011649118. doi:10.1073/pnas.2011649118
- Langmead, B., Trapnell, C., Pop, M., and Salzberg, S. L. (2009). Ultrafast and memory-efficient alignment of short DNA sequences to the human genome. *Genome Biol.* 10, R25. doi:10.1186/gb-2009-10-3-r25
- Li, W. Z., and Godzik, A. (2006). Cd-Hit: A fast program for clustering and comparing large sets of protein or nucleotide sequences. *Bioinformatics* 22, 1658–1659. doi:10.1093/bioinformatics/btl158
- Liedtke, H. C., Gower, D. J., Wilkinson, M., and Gomez-Mestre, I. (2018). Macroevolutionary shift in the size of amphibian genomes and the role of life history and climate. *Nat. Ecol. Evol.* 2, 1792–1799. doi:10.1038/s41559-018-0674-4
- Liu, X., Majid, M., Yuan, H., Chang, H., Zhao, L., Nie, Y., et al. (2022). Transposable element expansion and low-level piRNA silencing in grasshoppers may cause genome gigantism. *BMC Biol.* 20, 243. doi:10.1186/s12915-022-01441-w
- Love, M. I., Huber, W., and Anders, S. (2014). Moderated estimation of fold change and dispersion for RNA-seq data with DESeq2. *Genome Biol.* 15, 550. doi:10.1186/s13059-014-0550-8
- Luo, S., Zhang, H., Duan, Y., Yao, X., Clark, A. G., and Lu, J. (2020). The evolutionary arms race between transposable elements and piRNAs in *Drosophila melanogaster*. *BMC Evol. Biol.* 20, 14. doi:10.1186/s12862-020-1580-3
- Madison-Villar, M. J., Sun, C., Lau, N., Settles, M., and Mueller, R. L. (2016). Small RNAs from a big genome: The piRNA pathway and transposable elements in the salamander species *Desmognathus fuscus*. *J. Mol. Evol.* 83, 126–136. doi:10.1007/s00239-016-9759-3
- Malmström, M., Britz, R., Matschiner, M., Tørresen, O. K., Hadiaty, R. K., Yaakob, N., et al. (2018). The most developmentally truncated fishes show extensive Hox gene loss and miniaturized genomes. *Genome Biol. Evol.* 10, 1088–1103. doi:10.1093/gbe/evy058
- Matsuda, M., Nagahama, Y., Shinomiya, A., Sato, T., Matsuda, C., Kobayashi, T., et al. (2002). DMY is a Y-specific DM-domain gene required for male development in the medaka fish. *Nature* 417, 559–563. doi:10.1038/nature751
- Medstrand, P., Van De Lagemaat, L. N., and Mager, D. L. (2002). Retroelement distributions in the human genome: Variations associated with age and proximity to genes. *Genome Res.* 12, 1483–1495. doi:10.1101/gr.388902
- Meyer, A., Schloissnig, S., Franchini, P., Du, K., Woltering, J. M., Irisarri, I., et al. (2021). Giant lungfish genome elucidates the conquest of land by vertebrates. *Nature* 590, 284–289. doi:10.1038/s41586-021-03198-8
- Mueller, R. L. (2017). piRNAs and evolutionary trajectories in genome size and content. *J. Mol. Evol.* 85, 169–171. doi:10.1007/s00239-017-9818-4
- Nam, K., and Ellegren, H. (2012). Recombination drives vertebrate genome contraction. *PLoS Genet.* 8, e1002680. doi:10.1371/journal.pgen.1002680
- Novák, P., Guignard, M. S., Neumann, P., Kelly, L. J., Mlinarec, J., Kobližková, A., et al. (2020). Repeat-sequence turnover shifts fundamentally in species with large genomes. *Nat. Plants* 6, 1325–1329. doi:10.1038/s41477-020-00785-x
- Nowoshilow, S., Schloissnig, S., Fei, J.-F., Dahl, A., Pang, A. W. C., Pippel, M., et al. (2018). The axolotl genome and the evolution of key tissue formation regulators. *Nature* 554, 50–55. doi:10.1038/nature25458
- Orgel, L. E., and Crick, F. H. (1980). Selfish DNA: The ultimate parasite. *Nature* 284, 604–607. doi:10.1038/284604a0
- Ozata, D. M., Gainetdinov, I., Zoch, A., O'carroll, D., and Zamore, P. D. (2019). PIWI-Interacting RNAs: Small RNAs with big functions. *Nat. Rev. Genet.* 20, 89–108. doi:10.1038/s41576-018-0073-3
- Parhad, S. S., and Theurkauf, W. E. (2019). Rapid evolution and conserved function of the piRNA pathway. *Roy. Soc. Open Biol.* 9, 180181. doi:10.1098/rsob.180181
- Pasquesi, G. I. M., Perry, B. W., Vandewege, M. W., Ruggiero, R. P., Schield, D. R., and Castoe, T. A. (2020). Vertebrate lineages exhibit diverse patterns of transposable element regulation and expression across tissues. *Genome Biol. Evol.* 12, 506–521. doi:10.1093/gbe/evaa068
- Patro, R., Duggal, G., Love, M. I., Irizarry, R. A., and Kingsford, C. (2017). Salmon provides fast and bias-aware quantification of transcript expression. *Nat. Methods* 14, 417–419. doi:10.1038/nmeth.4197
- Perkins, R. D., Gamboa, J. R., Jonika, M. M., Lo, J., Shum, A., Adams, R. H., et al. (2019). A database of amphibian karyotypes. *Chromosome Res.* 27, 313–319. doi:10.1007/s10577-019-09613-1
- Price, A. L., Jones, N. C., and Pevzner, P. A. (2005). De novo identification of repeat families in large genomes. *Bioinformatics* 21 (1), i351–i358. doi:10.1093/bioinformatics/bti1018
- Reuter, M., Berninger, P., Chuma, S., Shah, H., Hosokawa, M., Funaya, C., et al. (2011). Miwi catalysis is required for piRNA amplification-independent LINE1 transposon silencing. *Nature* 480, 264–267. doi:10.1038/nature10672
- Rho, M., and Tang, H. (2009). MGEScan-non-LTR: Computational identification and classification of autonomous non-LTR retrotransposons in eukaryotic genomes. *Nucleic Acids Res.* 37, e143. doi:10.1093/nar/gkp752
- Rodriguez, F., and Arkhipova, I. R. (2018). Transposable elements and polyploid evolution in animals. *Curr. Opin. Genet. Dev.* 49, 115–123. doi:10.1016/j.gde.2018.04.003
- Rogers, R. L., Zhou, L., Chu, C., Márquez, R., Corl, A., Linderth, T., et al. (2018). Genomic takeover by transposable elements in the strawberry poison frog. *Mol. Biol. Evol.* 35, 2913–2927. doi:10.1093/molbev/msy185
- Said, I., Mcgurk, M. P., Clark, A. G., and Barbash, D. A. (2022). Patterns of piRNA regulation in *Drosophila* revealed through transposable element clade inference. *Mol. Biol. Evol.* 39, msab336. doi:10.1093/molbev/msab336

- Saint-Leandre, B., Capy, P., Hua-Van, A., and Filé, J. (2020). piRNA and transposon dynamics in *Drosophila*: A female story. *Genome Biol. Evol.* 12, 931–947. doi:10.1093/gbe/evaa094
- Senft, A. D., and Macfarlan, T. S. (2021). Transposable elements shape the evolution of mammalian development. *Nat. Rev. Genet.* 22, 691–711. doi:10.1038/s41576-021-00385-1
- Shannon, C. E. (1948). A mathematical theory of communication. *Bell Syst. Tech. J.* 27, 379–423. doi:10.1002/j.1538-7305.1948.tb01338.x
- Shen, W., Le, S., Li, Y., and Hu, F. (2016). SeqKit: A cross-platform and ultrafast toolkit for FASTA/Q file manipulation. *PLoS One* 11, e0163962. doi:10.1371/journal.pone.0163962
- Simao, F. A., Waterhouse, R. M., Ioannidis, P., Kriventseva, E. V., and Zdobnov, E. M. (2015). BUSCO: Assessing genome assembly and annotation completeness with single-copy orthologs. *Bioinformatics* 31, 3210–3212. doi:10.1093/bioinformatics/btv351
- Simpson, E. H. (1949). Measurement of diversity. *Nature* 163, 688. doi:10.1038/163688a0
- Sun, C., and Mueller, R. L. (2014). Hellbender genome sequences shed light on genomic expansion at the base of crown salamanders. *Genome Biol. Evol.* 6, 1818–1829. doi:10.1093/gbe/evu143
- Sun, C., Shepard, D. B., Chong, R. A., Arriaza, J. L., Hall, K., Castoe, T. A., et al. (2012). LTR retrotransposons contribute to genomic gigantism in plethodontid salamanders. *Genome Biol. Evol.* 4, 168–183. doi:10.1093/gbe/evr139
- Teefy, B. B., Siebert, S., Cazet, J. F., Lin, H., and Juliano, C. E. (2020). PIWI-piRNA pathway-mediated transposable element repression in Hydra somatic stem cells. *RNA* 26, 550–563. doi:10.1261/rna.072835.119
- Thomas, J. H., and Schneider, S. (2011). Coevolution of retroelements and tandem zinc finger genes. *Genome Res.* 21, 1800–1812. doi:10.1101/gr.121749.111
- Vandeweghe, M. W., Platt, R. N., Ray, D. A., and Hoffmann, F. G. (2016). Transposable element targeting by piRNAs in Laurasiatherians with distinct transposable element histories. *Genome Biol. Evolution* 8, 1327–1337. doi:10.1093/gbe/evw078
- Wang, J., Itgen, M. W., Wang, H., Gong, Y., Jiang, J., Li, J., et al. (2021a). Gigantic genomes provide empirical tests of transposable element dynamics models. *Genom. Proteom. Bioinform.* 19, 123–139. doi:10.1016/j.gpb.2020.11.005
- Wang, K., Wang, J., Zhu, C., Yang, L., Ren, Y., Ruan, J., et al. (2021b). African lungfish genome sheds light on the vertebrate water-to-land transition. *Cell* 184, 1362–1376.e18. doi:10.1016/j.cell.2021.01.047
- Wang, X., Ramat, A., Simonelig, M., and Liu, M.-F. (2023). Emerging roles and functional mechanisms of PIWI-interacting RNAs. *Nat. Rev. Mol. Cell Biol.* 24, 123–141. doi:10.1038/s41580-022-00528-0
- Warmuth, V. M., Weissensteiner, M. H., and Wolf, J. B. (2022). Accumulation and ineffective silencing of transposable elements on an avian W Chromosome. *Genome Res.* 32, 671–681. doi:10.1101/gr.275465.121
- Wei, K. H.-C., Gibilisco, L., and Bachtrog, D. (2020). Epigenetic conflict on a degenerating Y chromosome increases mutational burden in *Drosophila* males. *Nat. Commun.* 11, 5537–5539. doi:10.1038/s41467-020-19134-9
- Wei, K. H.-C., Mai, D., Chatla, K., and Bachtrog, D. (2022). Dynamics and impacts of transposable element proliferation in the *Drosophila nasuta* species group radiation. *Mol. Biol. Evol.* 39, msac080. doi:10.1093/molbev/msac080
- Wenke, T., Döbel, T., Sörensen, T. R., Junghans, H., Weisshaar, B., and Schmidt, T. (2011). Targeted identification of short interspersed nuclear element families shows their widespread existence and extreme heterogeneity in plant genomes. *Plant Cell* 23, 3117–3128. doi:10.1105/tpc.111.088682
- Wheeler, T. J., and Eddy, S. R. (2013). nhmmer: DNA homology search with profile HMMs. *Bioinformatics* 29, 2487–2489. doi:10.1093/bioinformatics/btt403
- Wicker, T., Sabot, F., Hua-Van, A., Bennetzen, J. L., Capy, P., Chalhoub, B., et al. (2007). A unified classification system for eukaryotic transposable elements. *Nat. Rev. Genet.* 8, 973–982. doi:10.1038/nrg2165
- Yang, G., Nagel, D. H., Feschotte, C., Hancock, C. N., and Wessler, S. R. (2009). Tuned for transposition: Molecular determinants underlying the hyperactivity of a stowaway MITE. *Science* 325, 1391–1394. doi:10.1126/science.1175688
- Zhang, J., Kobert, K., Flouri, T., and Stamatakis, A. (2014). Pear: A fast and accurate Illumina paired-end reAd mergeR. *Bioinformatics* 30, 614–620. doi:10.1093/bioinformatics/btt593
- Zhang, P., Kang, J. Y., Gou, L. T., Wang, J., Xue, Y., Skogerboe, G., et al. (2015). MIWI and piRNA-mediated cleavage of messenger RNAs in mouse testes. *Cell Res.* 25, 193–207. doi:10.1038/cr.2015.4
- Zhang, S., Pointer, B., and Kelleher, E. S. (2020). Rapid evolution of piRNA-mediated silencing of an invading transposable element was driven by abundant de novo mutations. *Genome Res.* 30, 566–575. doi:10.1101/gr.251546.119